

**INHIBITORY EFFECT OF SUBTHRESHOLD TRANSCRANIAL MAGNETIC  
STIMULATION ON THE STRETCH-EVOKED LONG LATENCY  
RESPONSE OF FOREARM MUSCLES**

by

Paria Arfa Fatollahkhani

A thesis submitted to the Faculty of the University of Delaware in partial fulfillment of the requirements for the degree of Master of Science in Biomechanics and Movement Science

Fall 2021

© 2021 Paria Arfa Fatollahkhani  
All Rights Reserved

**INHIBITORY EFFECT OF SUBTHRESHOLD TRANSCRANIAL MAGNETIC  
STIMULATION ON THE STRETCH-EVOKED LONG LATENCY  
RESPONSE OF FOREARM MUSCLES**

by

Paria Arfa Fatollahkhani

Approved: \_\_\_\_\_  
Fabrizio Sergi, Ph.D.  
Professor in charge of thesis on behalf of the Advisory Committee

Approved: \_\_\_\_\_  
Samuel Lee, Ph.D.  
Chair of the Department of Biomechanics and Movement Science

Approved: \_\_\_\_\_  
Kathleen S. Matt, Ph.D.  
Dean of the College of Health Sciences

Approved: \_\_\_\_\_  
Louis F. Rossi, Ph.D.  
Vice Provost for Graduate and Professional Education and  
Dean of the Graduate College

## ACKNOWLEDGMENTS

First, I would like to thank my advisor Dr. Fabrizio Sergi for giving me the opportunity of learning and challenging with such a novel interesting neuromodulation research field and extending my skills to the new world of biomechanics and robotic neurorehabilitation. I would like to also thank him for all his guidance and feedback throughout several stages of my projects and all the ups and downs of this master's journey.

Then, I would like to thank my committee members, Dr. Jared Medina and Dr. Joshua Cashaback, for supporting this work with their inputs, which definitely enhanced the scientific worth and quality of this thesis.

I am also grateful to all my colleagues and friends in the Human Robotics Lab, with special thanks to Andrea Zonnino and Andria Farrens for sharing their experience with me, throughout these years.

I also wish to express my warmest gratitude to all my friends near and far, with specific thanks to Taraneh, Farzaneh and Marjan for their extraordinary friendship which provided me relaxing moments and kept me motivated, and who are not only my close friends but also kind of my second family, far from home.

And my heartfelt appreciation goes to my family, my lovely parents, and siblings, for all their inspirations, patience and kindness which pass all this distance and are the main resources of motivation and faith to my goals all over my life.

## TABLE OF CONTENTS

LIST OF TABLES .....	vi
LIST OF FIGURES .....	vii
ABSTRACT .....	x
Chapter	
1 INTRODUCTION.....	1
1.1 Primary and secondary motor pathways.....	1
1.2 Role of motor pathways in long-latency responses .....	5
1.3 Using neuromodulation to decouple different pathways involved in long-latency responses .....	10
1.3.1 Neurophysiology of TMS.....	10
1.3.2 Previous uses of TMS to study the role of pathways involved in long-latency responses .....	13
1.4 Contribution of this work .....	18
1.5 Organization of the thesis.....	19
1.5.1 Part I: Developing a synchronized method for a simultaneous TMS stimulation and robotic perturbations which evoke LLRs from the forearm muscles, recorded by surface EMG .....	19
1.5.2 Part II: Quantifying the inhibitory effect of subthreshold TMS on the cortical contribution to LLRs measured in the forearm muscles .....	19
2 DEVELOPING A SYNCHRONIZED METHOD FOR A SIMULTANEOUS TMS STIMULATION AND ROBOTIC PERTURBATIONS WHICH EVOKE LLRs FROM THE FOREARM MUSCLES.....	21
2.1 Robotic perturbation system (neuromechanics) .....	21
2.2 EMG acquisition (neurophysiology) .....	22
2.3 Cortical TMS (neuromodulation) .....	25
2.3.1 Navigation processing .....	26
2.3.2 Stimulation processing .....	29
2.4 Determining the “cortical” motor threshold .....	30
2.5 Synchronization of robotic perturbations, TMS, and EMG .....	32

2.5.1	Example of synchronized robot-EMG-TMS .....	37
3	QUANTIFYING THE INHIBITORY EFFECT OF SUBTHRESHOLD TMS ON THE CORTICAL CONTRIBUTION TO LLRs MEASURED IN THE FOREARM MUSCLES.....	39
3.1	Materials and methods.....	39
3.1.1.1	Participants .....	40
3.1.2	Experimental procedures .....	40
3.1.2.1	Subject specific measurements.....	41
3.1.2.2	Perturbation Experiment.....	42
3.1.3	Data analysis.....	43
3.1.4	Statistical analysis .....	44
3.1.4.1	Group-level analysis .....	44
3.1.4.2	Subject-specific analysis .....	45
3.1.4.3	Repeatability analysis.....	45
3.1.5	Power analysis.....	45
3.2	Results .....	46
3.2.1	Subject specific measurements results .....	46
3.2.2	Observations from selected participants.....	48
3.2.3	Group-level analysis .....	53
3.2.4	Subject-level analysis .....	55
3.2.5	Repeatability analysis .....	59
4	CONCLUSIONS .....	60
4.1	Major findings .....	60
4.2	Future study .....	63
	REFERENCES .....	64
Appendix		
A	T1 STRUCTURAL SCAN REPORT .....	73
B	IRB/HUMAN SUBJECTS APPROVAL.....	75

## LIST OF TABLES

Table 1-1 List and details of previous studies evaluated the effects of TMS signal on the LLR amplitude.....	16
Table 3-1 Demographic and subject-specific measurement data of all subjects .....	47
Table 3-2 Dunnett’s test results with TMS Off- Pert On, group 1, control condition..	53
Table 3-3 Dunnett’s test results with TMS Off- Pert On, group 2, control condition..	54

## LIST OF FIGURES

Figure 1.1	Descending motor pathway through the corticospinal and reticulospinal tracts. The ipsilateral premotor (PM) and supplementary motor area (SMA), send inputs through the medial PMRF, which descends ipsilaterally. The excitatory descending inputs are provided to the spinal motor neurons via the medial cortico-reticulo-spinal tract (CRST). The contralateral primary motor cortex (M1) delivers inputs to the dorsolateral PMRF... ..	4
Figure 1.2	(A) EMG signal shows the long-latency muscle stretch reflex, as a burst of muscle activity occurring 50–100 ms following an imposed limb displacement. EMG: electromyography, nu: no unit, ms: millisecond, SLR: short-latency reflex, LLR: long-latency reflex, Vol: voluntary... ..	6
Figure 1.3	(A) Expected contribution of RF nuclei (shown in two axial sections at the level of the pons and medulla) to LLRs. (B) Activation maps measured by our group using StretchfMRI in the brainstem for the flexor carpi radialis (FCR) and extensor carpi ulnaris (ECU). Maps indicate LLR specific activity... ..	9
Figure 1.4	The TMS stimulation coil is located tangentially on the head and the magnetic field penetrates the scalp, which induces a secondary eddy current in the intracranial tissue. This electrical field is oriented perpendicular to the magnetic field with an opposite direction relative to the electrical current in the stimulation coil.. ..	11
Figure 2.1	Exploded (above) and prototype (bottom) views of the MR-StretchWrist robot. (1) Ultrasonic motor, (2) Output pulley, (3) Input pulley, (4) Tensioning mechanisms, (5) Structural bearings, (6) Force/Torque Sensor, (7) hand support... ..	22
Figure 2.2	A) BrainAmp EXG-MR amplifier. B) Placement of EMG electrodes on the forearm muscles... ..	23
Figure 2.3	Screenshots indicating two EMG recordings from the same subject during the same session. (Top), signal with large noise at the beginning of the acquisition session... ..	24
Figure 2.4	A) The MagPro X100 with MagOption stimulator B) The MCF-B65 Butterfly Coil, C) an image-based navigation system that includes reflective markers placed on the subject's forehead and a camera to enable localization of the coil over the stimulation region... ..	25

Figure 2.5	‘Entry’ (green) and ‘Target’ (red) points were set during the navigation processing as a guidance to localize the coil on the motor hot spot for forearm muscles. ....	27
Figure 2.6	‘Anterior commissure’ (yellow), ‘Posterior commissure’ (Pink) , and ‘cortical Falx point’ (blue) regions were set as the three main cortical connector areas between the two brain hemispheres.....	28
Figure 2.7	The pointer was driven side to side on the subject’s skull surface, indicated by the blue dots on the figure.....	29
Figure 2.8	The butterfly coil was located on the left (contralateral) motor cortex of the subject, guided by the ‘Entry’ and ‘Target’ points, were set in the navigation processing. ....	30
Figure 2.9	MEP evoked during AMT measurement from ECU muscle with a signal intensity of 45% MSO, which was followed by a SP on the EMG signal.....	32
Figure 2.10	The Simulink model which was used to generate the abovementioned signals to the TMS amplifier and the robot from the Q2-USB DAQ.....	33
Figure 2.11	The synchronized Robot-TMS-EMG system.. ....	34
Figure 2.12	The functional diagram of the synchronized Robot-TMS-EMG system. Different components and the transmitted signals are shown. ....	35
Figure 2.13	Timing diagram of the TMS pulse, the robotic perturbation, and MEP evoked on the active muscle. $T_1$ is the latency between TMS and MEP, $T_L$ is the desired MEP latency (relative to perturbation onset), and $\Delta T$ is the delay to achieve a desired $T_L$ . Following the MEP, there is a silent window of reduced motoneuron excitability, which we expected to result in a decrease of LLRa measured in response to perturbations.....	36

Figure 2.14	A) The motor-position and the normalized EMG activity recorded from the FCR muscle in conditions without a TMS pulse. The shaded area shows the evoked LLR activity window. B) The applied TMS trigger, the motor-position and the normalized EMG activity recorded from the FCR muscle for the same subject, when the TMS pulse was applied with 55ms delay ( $T_1(35) + T_L(20) = \Delta T = 55\text{ms}$ ) to the robot perturbation..	38
Figure 3.1	Subject seated on the chair with TMS coil placed on his left motor cortex and his right forearm placed in the hand support of robot, cued by a graphical interface on the laptop.....	41
Figure 3.2	A) plots of all experimental conditions for one subject from group 1 (90% AMT). Rectified EMG signal recorded from the FCR muscle, for 20 trials per condition, is illustrated in each plot. The shaded area is the LLR activity on EMG signal between 50-100ms after the stretch onset. The area under the curve within this shaded area was used as the LLRa measurement.....	50
Figure 3.3	A) plots of all experimental conditions for one subject from group 2 (95% AMT). Rectified EMG signal recorded from the FCR muscle, for 20 trials per condition, is illustrated in each plot. The shaded area is the LLR activity on EMG signal between 50-100ms after the stretch onset. The area under the curve within this shaded area was used as the LLRa measurement.....	52
Figure 3.4	Least square means plots. Each group five experimental conditions compared by its TMS off-Pert On condition (bars indicate the standard errors). The asterisks denote the significant results based on the Dunnett's test results. ....	55
Figure 3.5	The plots for distribution of LLRa for all the subjects in group 1, for three TMS application time delays conditions. Each line shows the range with the bolded region indicates the inter quartiles range centered on the median.....	57
Figure 3.6	The plots for distribution of LLRa for all the subjects in group 2, for three TMS application time delays conditions. Each line shows the range with the bolded region indicates the inter quartiles range centered on the median.....	58
Figure 3.7	Least square means plot for two experiment repetitions for subject 6. A significant reduction in LLRa was measured in day 2 compared to day 1 of the experiment. ....	59

## ABSTRACT

The central nervous system controls human movements using multiple pathways that relay neural input to the muscles. The reticulospinal tract (RST) is a prominent secondary motor pathway, as it extends the function of the primary motor pathway, the corticospinal tract (CST). The RST is especially important for its involvement in locomotion, maintenance of posture, reaching, and grasping, which has considerable importance for recovery from corticospinal lesions such as stroke. There is currently a debate on whether increased reticulospinal function is necessary for recovery of motor function after severe lesions of the CST, or a sign of maladaptive plasticity. A primary reason for the unresolved debate is the lack of methods for measuring function of the reticular formation, a collection of nuclei in the brainstem that originate the RST.

An important component of upper limbs movement mechanisms is the “long-latency response” (LLR), which is evident as a burst of muscle activity occurring 50–100 ms following an imposed limb displacement. Although the neural processing of these long latency responses through the cortical circuits has been roughly distinguished, it is still unclear how the RST circuits contributes to the LLR, independently from the cortical inputs. A possible method for decoupling the contribution of the CST and the RST to LLR would be to use the inhibitory TMS neuromodulation. Previous studies utilized TMS to study the neural substrates of LLR, demonstrating that the effects of TMS signal delivered over the motor cortex on the LLR amplitude (LLRa) are modulated by the signal intensity and arrival time relative to the EMG activity period. However, previous studies reported inconsistent findings of the effects of TMS on LLRa, reporting inconsistent inhibitory and excitatory LLR

modulation. As such, the primary objective of this work was to develop a synchronized stimulation method including robotic perturbations, transcranial magnetic stimulation (TMS), and surface electromyography (EMG), which would allow to decouple the contributions of cortical and subcortical brain areas to LLRs.

In part I, we present our developed novel synchronized Robot-TMS-EMG method which produces TMS pulses of controllable magnitude and timed to induce a motor-evoked response (MEP) at controlled time delays relative to the application of robotic perturbations of the wrist joint, while the LLRs are recorded from the muscles by surface EMG electrodes. In part II, we present the results of our experiments on 13 young healthy participants to quantify the effects of subthreshold TMS over the motor cortex, on two groups of healthy subjects, with two intensities of 90% and 95% AMT, which was applied with three different time delays for each group, as  $T_1$  (which induced MEPs evoked at the same time as the robot perturbations started),  $T_2$  ( $T_1+20\text{ms}$ ), and  $T_3$  ( $T_1+50\text{ms}$ ), on the amplitude of LLRs recorded through surface EMG signals from FCR muscle, which was stretched through the wrist extension perturbations.

Our results identified two conditions ( $T_2$  and  $T_3$ ) that induced a significant inhibition of LLR activity in both groups, but no significant difference between groups was measured for any TMS delay levels inducing significant inhibition. Specifically, the  $T_2$  and  $T_3$  conditions resulted in a significant reduction of LLR amplitude (90% AMT group,  $T_2$ : 20.3%,  $p=0.008$ ;  $T_3$ : 22.8%,  $p=0.002$  – 95% AMT group,  $T_2$ : 15.1%,  $p=0.017$ ;  $T_3$ : 25.3%,  $p<0.001$ ), while condition  $T_1$  resulted in non-significant modulation of LLR amplitude (90% AMT group: 14.1% reduction,  $p=0.102$ ; 95% AMT group: 3.5% increase,  $p=0.912$ ). Moreover, TMS application which is timed to evoke MEPs 50ms before the stretch onset (condition  $T_3$ ) was found to have a greater

inhibitory effect on the LLRa in both groups, with both the 90% and 95% subthreshold TMS intensity. This time delay condition likely inhibited the intracortical pathways contributed to the LLRa, which is a crucial finding to be applied for our future TMS-fMRI study, which, for the first time, would be the demonstration of a successful combination of TMS and fMRI to study causality of neural function in a distributed motor circuit, involving the primary motor cortex and the brainstem, with the aim of understanding and measuring the specific contribution of the RST to the long-latency responses.

# Chapter 1

## INTRODUCTION

### 1.1 Primary and secondary motor pathways

The central nervous system controls human movements using multiple pathways that relay neural input to the muscles. The corticospinal (CST) pathway is the principal motor pathway for controlling movements that affords the greatest skill and flexibility required for fine motor control [1]. There are several pathways that contribute with the corticospinal tract to control motor actions, such as rubrospinal and reticulospinal tracts. The rubrospinal tract contributes to the finger movements via the monosynaptic connections to the innervating motoneurons of the distal muscles [2]. The reticulospinal tract (RST) controls both proximal and axial muscles, and its role in the control of gross movements, such as locomotion, reaching, and posture regulation has been clearly established [2]–[5].

The RST has considerable importance for recovery from corticospinal lesions such as stroke. There is currently a debate on whether increased reticulospinal function is necessary for recovery of motor function after severe lesions of the CST (positive role of RST in post-stroke recovery [6]–[9]) or a sign of maladaptive plasticity (negative role of RST in post-stroke recovery [10]–[13]). A primary reason for the unresolved debate is the lack of methods for measuring function of the reticular formation, a collection of nuclei in the brainstem that originate the RST.

In more details, there are two RS tracts which originate from different regions of the brainstem. The dorsolateral reticular formation located in the medulla, is the origin of the dorsal RST, which receives facilitatory inputs from the motor cortex through the corticoreticular fibers. The cortico-reticulospinal tract and lateral CST descend adjacently, at the spinal level, through the dorsolateral funiculus. The pontine tegmentum of the Pontomedullary reticular formation (PMRF) is the origin of the medial RST. The vestibulospinal tract (VST) and the medial RST descend together in the ventromedial cord. The inhibitory effects to the spinal reflex circuits are provided through the dorsal RST; however, the excitatory inputs are delivered through the medial RST and VST. Hence, in healthy subjects, a balanced excitatory and inhibitory neural drive are provided through the medial and lateral RSTs to the spinal motor neuron circuits [14]. In more details, evidence also suggested that via the internuncial (connector) neurons, the medial RST is responsible for extensor motor neurons (excitatory effects on the extensors and inhibitory effects on the flexor), while the lateral (dorsal) RST is responsible for flexor motor neurons (excitatory effects on the flexors and inhibitory effects on the extensors) [15]–[17].

Moreover, previous investigations demonstrated that there is a bilateral mutual organization in the motor activity of the RF, as the RF nuclei deliver excitation to the ipsilateral flexors and contralateral extensors; however, these nuclei provide inhibition to the contralateral flexors and ipsilateral extensors [8], [18], [19]. Animal studies which evaluated the in-vivo single-unit neural recordings of the PMRF nuclei in monkeys performing arm reaching tasks suggested a functional division of the two RSTs [18], [8], with the medial RST provides excitatory inputs to the extensors and inhibitory

inputs to the flexors, while the lateral (dorsal) RST delivers inhibition to the extensors and excitation to the flexors [19], [5].

In stroke, as the leading cause of motor disability [20], with cortical and internal capsular impairments, the CST pathway and the corticoreticular tract are mainly damaged as these pathways are anatomically close. Therefore, the facilitatory medial RST and VST pathways are leaved unopposed, followed by a hyperexcitability of these pathways [14], [21]–[24] (Fig 1.1). However, because of the technical complications, even with the recent most innovative technologies, functions of the brainstem nuclei and RST excitability has not yet been evaluated directly in the stroke survivors [14], [25]–[28].

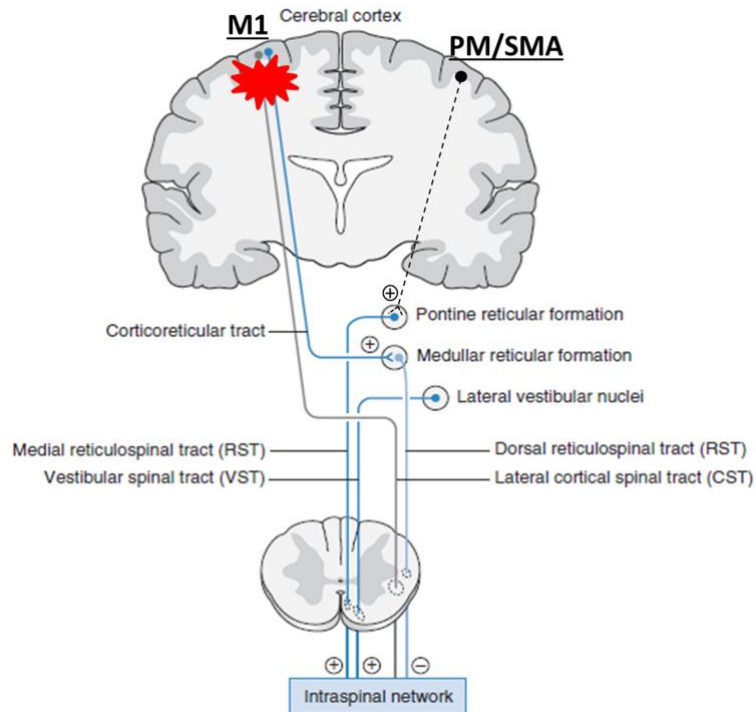


Figure 1.1 Descending motor pathway through the corticospinal and reticulospinal tracts. The ipsilateral premotor (PM) and supplementary motor area (SMA), send inputs through the medial PMRF, which descends ipsilaterally. The excitatory descending inputs are provided to the spinal motor neurons via the medial cortico-reticulo-spinal tract (CRST). The contralateral primary motor cortex (M1) delivers inputs to the dorsolateral PMRF. Inhibitory inputs are delivered to the spinal motor circuits through the dorsal CRST. Following the stroke, the output signals from the corticospial tract (CST) and CRST are reduced as these tracts are impaired on one hemisphere (indicated by a red asterisk). Therefore, the spinal motor neurons become hyperexcitable, or might be suddenly fired as a result of the hyperexcitation in the medial CRST of the contralesional hemisphere. (+) indicates excitatory and (-) indicates inhibitory effect [14]. The figure is adapted and modified from [29].

## **1.2 Role of motor pathways in long-latency responses**

An important component of upper limbs movement mechanisms is the “long-latency response” (LLR). The LLR is evident as a burst of muscle activity happening 50–100 ms following an imposed limb displacement. This response is observed between the short-latency reflex (SLR) occurs between 20–50 ms as the fastest response via the nervous system and the delayed voluntary reaction (after 100 ms) [30].

The SLR is generated by the monosynaptic spinal circuits through the group I afferent input as the only fast and short enough pathway to responsible. However, The LLR is induced by processing of group I afferent inputs through spinal [31]–[35] and supraspinal networks in addition to the spinal processing of group II afferent inputs [36]–[38]. A more distributed network consists of the premotor cortex and basal ganglia along with the faster circuits are involved in the voluntary reactions (Fig 1.2) [39], [40].

Multiple supraspinal circuits are involved in the LLR origination. There is a body of evidence indicates that M1 contributes to the LLR, which is highly innervated by the somatosensory inputs through the dorsal column pathway [41] and results in the quick activation to the perturbations of several joints as the wrist, elbow, or shoulder [39], [42], [43]. Furthermore, these M1 neurons with a fast response to limb perturbations also contribute to the LLR via connections, which directly synapse onto spinal motor neurons [44], [45].

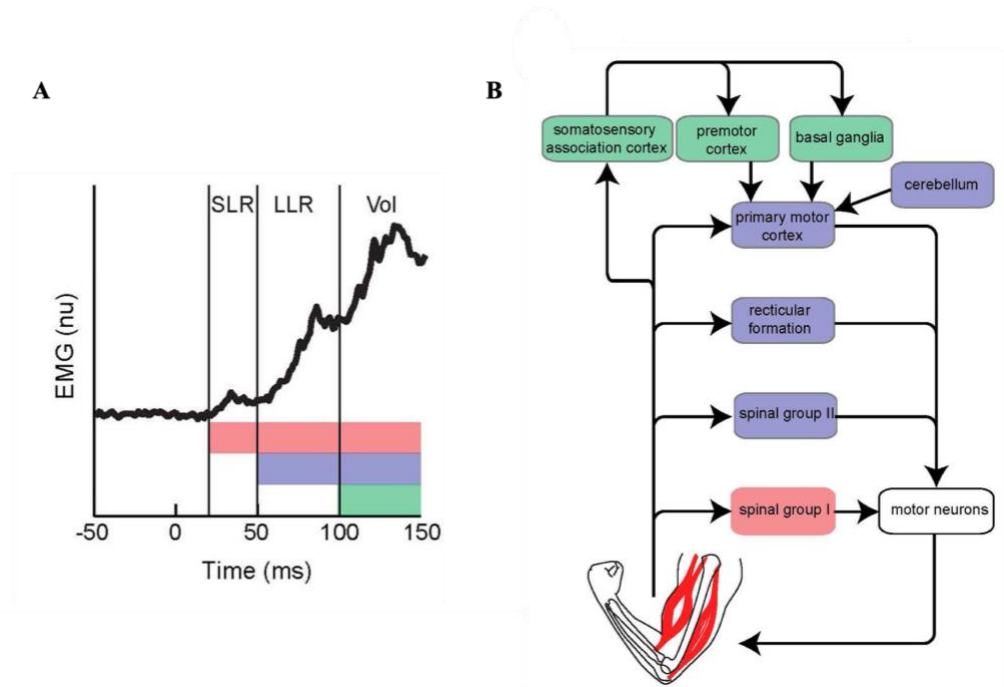


Figure 1.2 (A) EMG signal shows the long-latency muscle stretch reflex, as a burst of muscle activity occurring 50–100 ms following an imposed limb displacement. EMG: electromyography, nu: no unit, ms: millisecond, SLR: short-latency reflex, LLR: long-latency reflex, Vol: voluntary. (B) Simplified diagram of the neural substrates of the different epochs of the stretch-evoked muscle activity. The figure is adapted from [30].

Although the neural processing of these long latency responses through the cortical circuits has been roughly distinguished, it is still unclear how the RST circuits, which originates in the pontomedullary portion of the reticular formation (RF) region of brainstem, contributes to the LLR, independently from the cortical inputs.

Studies examined LLR responses evoked by postural perturbation to the elbow joint, demonstrated that larger LLR responses occur when subjects attempt to “resist” a perturbation than “yield” to the perturbation [46]. This observed task-dependent change

in LLR activity is the result of the temporal overlap of two distinct responses, a task-dependent response, and an automatic response [47]–[49]. Accumulating evidence indicated that RF is a candidate for generation of the task-dependent response [30], [49].

There are also evidence suggesting a relation between the LLR's task-dependency and the 'StartReact' phenomenon. StartReact is the ultra-fast release of a planned action cued by a startling stimulus (a loud auditory stimulus, 120 dB) [50], [51]. The faster than normal reaction (70 ms vs >100ms for arm muscles) after the startling stimulus likely reflects the involvement of RF and brainstem pathways [52]. Studies also showed that cortical stroke [53] and degenerated corticospinal tract patients [54] have normal onset of StartReact, while they have delayed voluntary movements. A study conducted in 2013, also demonstrated that a limb perturbation and a loud startling sound can induce similar pattern of activity in LLR EMG signal. Based on the similar muscle responses evoked by perturbations and the responses evoked by startling acoustic stimuli, it has been suggested that the perturbation-evoked early initiation of a planned motor action is likely to be generated at least partially by the startle neural network in the brainstem [55]. There are only some animal investigations suggesting the involvement of the reticular formation in the startle circuits [56]–[58]; however, there is a lack of direct evidence for this contribution in humans, and the available knowledge is also limited in the regional specificity.

Our group has developed a novel technique, StretchfMRI, which is capable of studying RST function associated with LLRs in-vivo in humans. StretchfMRI combines robotic perturbations with electromyography and fMRI to simultaneously quantify muscular and neural activity during LLRs. Using StretchfMRI, our group has the first-ever evidence of motor-related activation in the brainstem and established the muscle-

specific organization of LLR activity in the RF [59], [60]. The observed organization is partially consistent with previous knowledge derived from animal models, with activity primarily in the right medulla for flexors, and in the left pons for extensors [5], [8], [18], [19]. With StretchfMRI, we were able to observe activations also in other areas, such as the midbrain and bilateral pontomedullary contributions (Fig 1.3) [60].

It is noteworthy to consider that since the StretchfMRI uses fMRI to measure neural function, it cannot provide insight on the causality of the relationship between neural function and observed behavior. Specifically, the activations measured in the RF may, at least in part, be due to increased output from the primary motor cortex to the RF that occurs simultaneously with LLRs. As such, StretchfMRI cannot rule out the hypothesis that the RST only serves as a relay between the primary motor cortex and muscles, whereby cortical input would still be necessary for producing physiological LLRs.

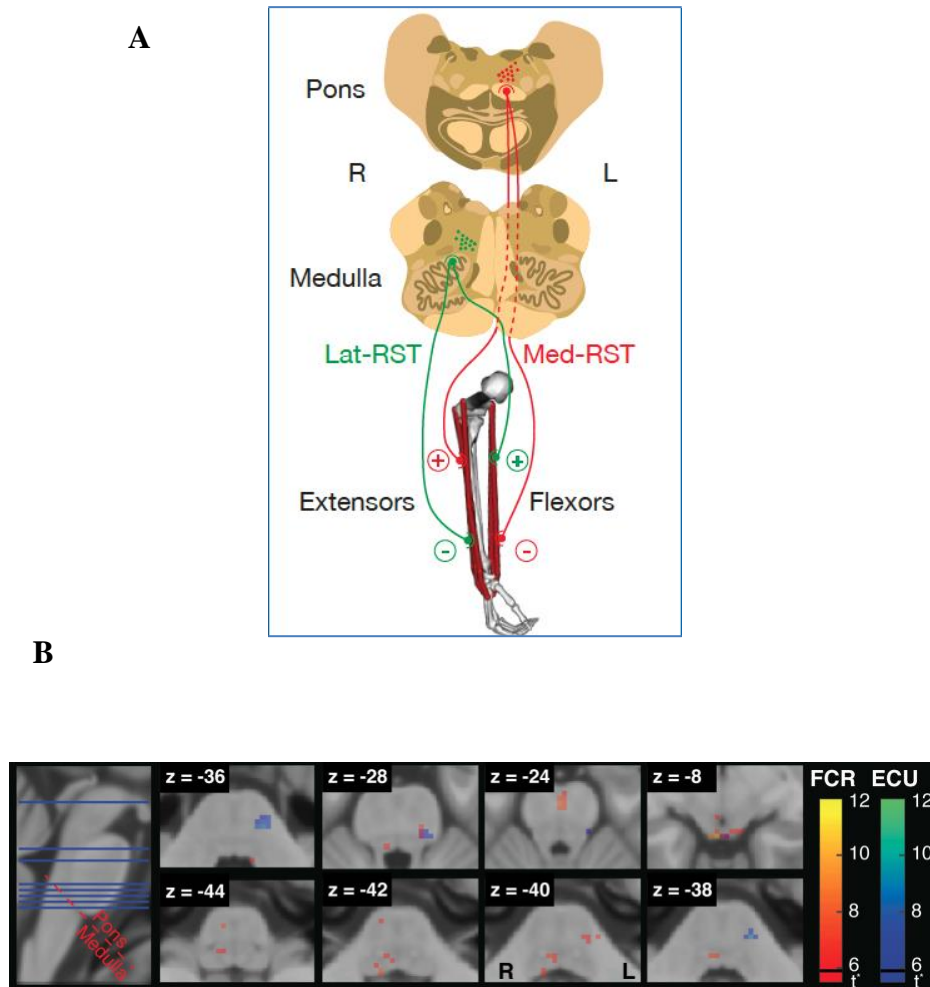


Figure 1.3 (A) Expected contribution of RF nuclei (shown in two axial sections at the level of the pons and medulla) to LLRs. (B) Activation maps measured by our group using StretchfMRI in the brainstem for the flexor carpi radialis (FCR) and extensor carpi ulnaris (ECU). Maps indicate LLR specific activity. All statistical parametric maps are overlaid on axial slices of the MNI-152 template, with reported z coordinate in mm. The figure is adapted from [60].

### **1.3 Using neuromodulation to decouple different pathways involved in long-latency responses**

#### **1.3.1 Neurophysiology of TMS**

TMS activates the cortical neurons making use of electromagnetic induction [61]. The TMS stimulator is discharged inducing a strong time-varying magnetic field to the coil. The stimulation coil is located tangentially on the head and the magnetic field gets through the scalp with minimal attenuation, which induces a secondary eddy current in the intracranial tissue. This electrical field is oriented perpendicular to the magnetic field with an opposite direction relative to the electrical current in the stimulation coil [62]. The induced electrical current runs parallelly to the TMS coil plane, through a medium with homogeneous conductivity (Fig 1.4). However, since the human brain does not have a homogeneous conductivity and the induced intracranial currents and their pathways are affected by the regional variations in tissue conductivity, extensive modeling is needed to predict the exact current distributions, considering the electrical properties of the tissue in the surrounding area of the coil [63].

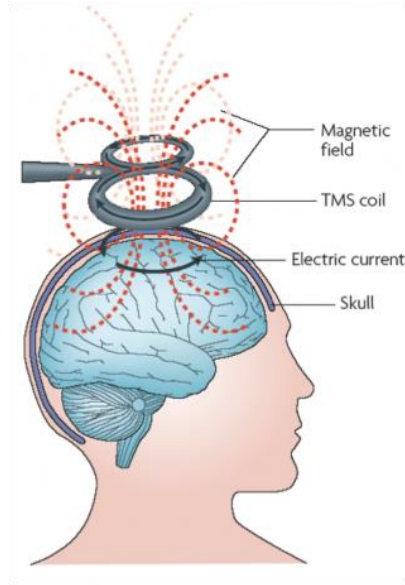


Figure 1.4 The TMS stimulation coil is located tangentially on the head and the magnetic field penetrates the scalp, which induces a secondary eddy current in the intracranial tissue. This electrical field is oriented perpendicular to the magnetic field with an opposite direction relative to the electrical current in the stimulation coil [62]. This figure is adapted from [64].

In order to stimulate the cortical neurons effectively, an outward directed trans-membrane current (ion flow) in cortical axons is needed to be produced by the current flow in the tissue, which will be resulted in a sufficiently strong ion flow to depolarize the membrane potential, followed by triggering an action potential. These induced electric field and the resultant cortical current flow are comparative to the rate of alteration (as the temporal derivative) in the induced electromagnetic field. Moreover, the efficacy of TMS to produce action potentials in cortical neurons is determined by the spatial relationship between the resultant tissue current and the stimulated axons (as the spatial derivative). Effective membrane depolarization will preferentially occur at regions where there is a maximal temporal and spatial derivatives of the induced

electrical field [62]. The axonal bendings have been found as an important spatial characteristic that indicates the susceptibility of cortical neurons to the TMS signals [65]: the TMS induced electric current leads to the transmembrane depolarization with an outward direction in susceptible axons within the field. Those axons which change their orientation relative to the resultant electric field are the most likely to be activated [65]. The action potentials induced in cortical axons by TMS pulses spread through synapses with other neurons, delivering a distribution of neuronal activation to connected cortical and subcortical regions [62], [66]. This volley of excitation descends through the corticospinal tract and peripheral motor nerve inducing muscle responses which can be recorded as motor evoked potentials (MEPs) [62].

These MEPs are recorded in order to determine two main motor-related cortical thresholds of resting motor threshold (RMT) and active motor threshold (AMT), which are determined while the target test muscle is at rest or during a slight tonic contraction of the target muscle, respectively [67]. The AMT indicates closely the threshold for inducing descending neural drive in the corticospinal tract's fast-conducting neurons, which is justifiable as the initial recruited descending volleys can effectively discharge those spinal motoneurons with an approximate firing threshold in an active condition [62], [67].

Notably, it is also evident that a duration of EMG silence of around 100 ms can be induced in a contracting muscle via the intense stimulation of its peripheral motor nerve [68]–[71], a phenomenon that we will here refer to as “silent period” induced by TMS stimulation. For a review of this concept and an in-detail description of its neurophysiological bases, please refer to these articles [70], [71]. We will here provide a synthetic account of this phenomenon, as it is crucial for the development of our

protocol and interpretation of the results. The ‘silent period’ (SP) can be justified by various mechanisms including withdrawal of Ia facilitatory effect to the motoneurons while the muscle is shortened because of the muscle twitch, which lasts relatively to the duration of the silent period [68]–[70]. A recurrent inhibition, and activation of Ib and cutaneous afferents which inhibited the motoneurons can also be induced by the antidromic volley in motor axons that blocks the ongoing neural drive, which can be the other possible underlying mechanisms [68]. Studies also demonstrated that the TMS delivered over the motor cortex during a muscle voluntary contraction also induces an EMG silent period which can last up to 300 ms. The silent period happens right after the excitatory motor evoked potential, and its duration is relative to the stimulation intensity [71], [72]. Importantly, the first 50 ms is widely considered to be induced due to the spinal inhibitory network, via mechanisms such as following of the hyperpolarization of the motoneurons and recurrent inhibition, but the further section of the silent period is assumed to be due to supraspinal inhibition [71]–[75]. This prolonged loss in the motor cortical output is resulted due to the activation of long-lasting GABA(B) mediated inhibition via the TMS [76], [77].

### **1.3.2 Previous uses of TMS to study the role of pathways involved in long-latency responses**

Previous studies utilized TMS to study the neural substrates of LLR, demonstrating that TMS can modulate the LLR amplitude (LLRa) in different ways depending on the TMS signal intensity and arrival time based on the EMG activity period.

Given that TMS signal intensity is mainly determined based on the AMT of the targeted muscle, previous studies utilized sub or suprathreshold TMS modulation on

LLRa [78]–[84]. Previous works demonstrated that TMS pulses over the motor cortex, may activate both the facilitatory and inhibitory cortical structures. Notably, evidence showed that the activation threshold for the magnetic stimulation is lower for the intracortical inhibitory circuits in comparison to the corticospinal cells, which are activated by a higher and suprathreshold stimulus intensities [85], [86]. Therefore, subthreshold TMS delivered to M1 has been shown to be able to activate intracortical inhibitory structures and does not elicit any descending volleys in the corticospinal tract. Findings suggested that subthreshold TMS changes the motoneuron pool excitability, without eliciting a direct muscle response [82], [86].

Several previous studies targeting the effects of subthreshold TMS on LLR reported non-coherent excitatory and inhibitory effects of subthreshold TMS on the LLR amplitude, but agreed that there was a significant effect of TMS pulse timing on whether the effect would be facilitatory or excitatory [78], [80], [82], [84]. Specifically, Doornik et al., 2004 [82], showed that the TMS signal with 90% of AMT over the motor cortex had an inhibitory effect on the LLRa evoked from the tibialis anterior muscle, when TMS was administrated 55–85 ms prior to LLR onset. On the other hand, another study in 2004 [80], reported a reduction in the LLR amplitude while TMS signal over the motor cortex was timed to induce an MEP at the SLR onset of the EMG activity, which was recorded from the flexor carpi radialis (FCR) muscle. This inhibition was increased as the TMS signal increased from 90% to 140% AMT. Moreover, two other studies also evaluated how a subthreshold TMS signal over the motor cortex would modulate the LLRa evoked from FCR muscle when the extension perturbations were applied on the wrist joint [78], [84]. While the abovementioned studies mainly demonstrated the M1 and intracortical pathways contribution to the LLRs, there were

also studies with TMS application timing, which shows the spinal circuits contribution to the LLRs. Ruit et al., in 2011 [84], observed both excitatory and inhibitory effects of a subthreshold TMS signal 2-3% below the AMT on the FCR LLRa. Signals which arrived within 35 to 55 ms (average of 45 ms) after the stretch onset inhibited the LLRa, while signals with averaged arrival time of 60 ms after the stretch onset, excited the LLRa. The other study in 2015 [78], reported no inhibitory, but excitatory effects of a subthreshold TMS signal with an intensity of 96% below the AMT on the LLRa evoked from FCR muscle. These authors also found that the TMS pulses which were timed to evoke MEPs within 60 to 90 ms after the stretch onset substantially augmented the FCR evoked LLR activity.

Furthermore, some studies also investigated the LLR neural pathways through the modulation of task instructions [79], [81]. Studies examined LLR responses evoked by postural perturbation to the elbow joint, demonstrated that larger LLR responses occur when subjects attempt to “resist” a perturbation than “yield” to the perturbation [46], [87]. Researchers suggested that this observation is likely to be attributed to the task-dependent change in LLR activity. In addition, the task-dependent change in LLR activity is the result of the temporal overlap of two distinct responses, a task-dependent response, and an automatic response [47]–[49]. Accumulating evidence indicated that RF is a candidate for generation of the task-dependent response [30], [49].

In this regards, one study showed that transient suppression of M1 by a suprathreshold TMS pulse, applied 50 ms before the elbow joint perturbation, does not diminish the LLR amplitude during the “resist” instruction, while the TMS pulse inhibited the LLR amplitude when the subjects did not intervene (DNI) to the perturbations. This observation suggests that substrates other than M1 are responsible

for the increase in LLR signal measured when the task instruction is to “resist” the perturbation, compared to when the instruction is to “yield” to ” the perturbation [81]. Meziane et al, also showed that LLRs are larger when subjects compensate (resist) to the perturbations; they also applied TMS pulses at 100% RMT intensity, which resulted in inhibition in the LLR amplitude while subjects did not intervene to the perturbations, which wasn’t observed with the compensation instruction [79].

The abovementioned previous TMS investigations on the neural pathways of LLRs are summarized and detailed in the table below.

Table 1-1 List and details of previous studies evaluated the effects of TMS signal on the LLR amplitude

	Shemmell 2009	Doornik 2004	Meziane 2009	Ruit 2011	Lewis 2004	Perenboom 2015
Joint	Elbow	Ankle	Wrist	Wrist	Wrist	Wrist
Stretched Muscle	Biceps Brachii	Tibialis Anterior	Flexor Carpi Radialis	Flexor Carpi Radialis	Flexor Carpi Radialis	Flexor Carpi Radialis
Instruction	DNI, Resist	DNI	NINT, COMP	DNI	DNI	DNI
Coil and Stimulator type	Figure-8 MagStim 200	Figure-8 MagStim200	Figure-8 MagStim 200	Figure-8 MagStim Rapid 2	Figure-8 MagStim 200	Figure-8 MagStim Rapid 2
Sub/Supra Threshold	Supra	Sub	Supra	Sub	Sub + Supra	Sub
Intensity	163±14% of AMT	90% of AMT	100% of RMT	97-98% of AMT	90, 100, 110, 120, 130, and 140 of AMT	96% of AMT

TMS application Time (relative to stretch onset)	50 ms before stretch Onset	-60 ms to +100 ms to stretch Onset	0.5-1.5 s before stretch Onset	35– 80ms after stretch onset	5– 35ms after stretch onset	25–70 ms after stretch onset
Time of evoked MEP peaks (relative to stretch onset)	-33ms	-28 to +132ms	-1483 to -483ms	52 to 97ms	22 to 52ms	42 to 87ms
Effect on LLRa	INH	INH	INH	INH+EXC	INH	EXC
Results	INH: with DNI instruction  Larger LLRa with resist vs. DNI	INH: TMS application 55–85 ms prior to LLR onset  Average d LLR onset: (99±8 ms after stretch onset)	INH: with NINT instruction  Larger LLRa with COMP vs. NINT	INH: TMS application at 45ms (35-55) EXC: TMS application at 60ms	INH: TMS induced MEPs at SLR onset  LLRa decreased as TMS intensity increased	EXC: TMS induced MEPs between 60 and 90 ms after stretch

DNI, NINT: (Do) not to intervene, COMP: compensate, AMT: active motor threshold, RMT: resting motor threshold, INH: inhibitory, EXC: excitatory, TMS: transcranial magnetic stimulation, SLR: short-latency reflex, LLR: long-latency response, LLRa: long-latency response amplitude, MEP: Motor evoked potential. ‘Time of evoked MEP peaks (relative to stretch onset)’ was calculated based on the averaged MEP latency for upper extremities as 17ms [88] and lower extremities as 32ms [89].

#### **1.4 Contribution of this work**

This long-term goal of this research is to improve our understanding of the neural processing of long-latency responses (LLR), specifically the contribution of secondary pathways to long-latency responses. While previous studies utilized different TMS signal intensity and timing protocols, there are controversial findings and scarce data on the appropriate intensity and arrival time of TMS signal for a cortical inhibition. Furthermore, based on the best of our knowledge, there is no prior study used subthreshold TMS to achieve inhibition on the LLR amplitude by relying primarily on the intracortical inhibitory effects of TMS via a silent period, with consideration of the first 50 ms spinal and following intracortical neurophysiology of silent period phenomenon to manipulate the TMS application timing, which was one of our main objectives in development of our synchronized robotic TMS-EMG system. Notably, this combination of subthreshold TMS and silent-period inhibition would be ideal to study subcortical contributions via fMRI in a future study.

In this work, we seek to apply a subthreshold TMS signal which has been shown to be able to activate intracortical inhibitory structures and does not elicit any descending volleys in the corticospinal tract [82], [86]. We found this feature of subthreshold TMS signal crucial to be considered in our work as the findings of this thesis project will be used in our future TMS-fMRI study which, for the first time, would be the demonstration of a successful combination of TMS and fMRI to study causality of neural function in a distributed motor circuit, involving the primary motor cortex and the brainstem. These methods will be enabled utilizing our novel MR-compatible TMS device for the neuromodulation of motor circuits, which, for the first time, enables the combination of these two methods. The application of the new methods will generate new knowledge on the neural processing of long-latency muscle responses. Specifically,

the identification of a causal link between neural circuits and behavior is considered one of the most important topics of investigation of modern neuroscience [90]. Causal knowledge on neural function is crucial to assess the ubiquitous what-if scenarios that are so important in stroke research, such as “in absence or reduction of cortical input, can the reticular formation positively contribute to recovery of motor function?”, targeted with the continuation of this study.

## **1.5 Organization of the thesis**

We present our work in two distinct parts, as outlined below:

### **1.5.1 Part I: Developing a synchronized method for a simultaneous TMS stimulation and robotic perturbations which evoke LLRs from the forearm muscles, recorded by surface EMG**

In chapter 2, we present our developed method which produces TMS pulses of controllable magnitude and timed to induce a motor-evoked response (MEP) at controlled time delays relative to the application of robotic perturbations of the wrist joint, while the LLRs are recorded from the muscles by surface EMG electrodes.

### **1.5.2 Part II: Quantifying the inhibitory effect of subthreshold TMS on the cortical contribution to LLRs measured in the forearm muscles**

In chapter 3, we present the results of our experiments on 12 young healthy participants to validate our novel experimental setup comprising of TMS stimulation, robotic perturbations, and surface EMG. The goal of these experiments was to identify parameters of TMS stimulation that inhibit the contribution of the primary motor cortex to LLRs. In this aim, we targeted the following performance metric: the amplitude and

delay of TMS pulse stimuli can be tuned to achieve an inhibition in LLR amplitude in healthy participants in the forearm muscles.

In chapter 4, we present the discussion and conclusion of this project findings on the inhibitory effects of the subthreshold TMS pulses over the motor cortex, synchronized through our Robotic-TMS-EMG method, on the stretch-evoked LLR amplitude measured in the forearm muscles.

## Chapter 2

### **DEVELOPING A SYNCHRONIZED METHOD FOR A SIMULTANEOUS TMS STIMULATION AND ROBOTIC PERTURBATIONS WHICH EVOKE LLRs FROM THE FOREARM MUSCLES**

This project contains three main dimensions of ‘Neurophysiology’, ‘Neuromechanics’, and ‘Neuromodulation’. We developed a method integrating these three dimensions to synchronize the application of a wrist perturbation via a robot (neuromechanics) with the acquisition of surface electromyography from forearm muscles (neurophysiology), with the application of transcranial magnetic stimulation pulses to the primary motor cortex (neuromodulation). These methods and equipment are detailed in separate sections below.

#### **2.1 Robotic perturbation system (neuromechanics)**

Our group has previously developed the MR-StretchWrist, a robot capable of applying velocity-controlled perturbations to the wrist in flexion and extension and evoke stretch-related responses in forearm muscles (Fig. 2.1) [59]. The MR-StretchWrist is the only MRI-compatible device that can be used to elicit velocity controlled stretch responses enabling the study of their neural correlates using fMRI. The MR-StretchWrist is a single degree of freedom robot designed to support movements of the wrist about the flexion/extension axis, with a range of motion of 90 deg. The MR-StretchWrist is actuated by an ultrasonic piezoelectric motor (EN60 motor, Shinsei Motors Inc., Japan), which provides 1 Nm peak torque and 900 deg/s peak velocity. To increase the torque output, we have employed a capstan transmission with a 3:1 gear ratio to transfer motion from the motor to the end effector. The MR-

StretchWrist is instrumented with a six-axis MR-compatible Force/Torque sensor (Mini 27Ti, ATI Industrial Automation, Apex, NC, and by an incremental encoder mounted on the motor shaft (US Digital, resolution: 0.06 deg) to measure the torque and rotation, respectively, of the wrist joint about the flexion/extension axis. The MRI compatibility of the MR-StretchWrist has been demonstrated in prior work [59].

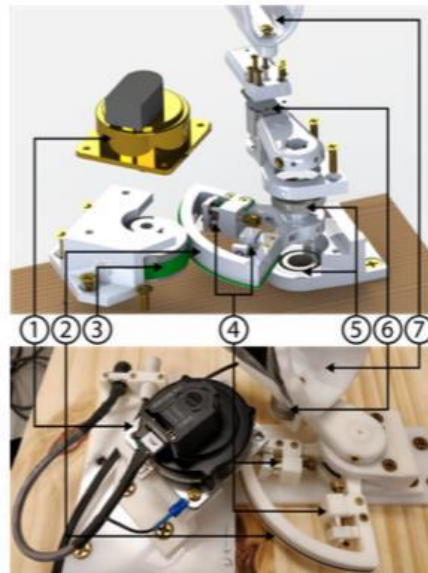


Figure 2.1 Exploded (above) and prototype (bottom) views of the MR- StretchWrist robot. (1) Ultrasonic motor, (2) Output pulley, (3) Input pulley, (4) Tensioning mechanisms, (5) Structural bearings, (6) Force/Torque Sensor, (7) hand support. Figure is adapted from [59].

## 2.2 EMG acquisition (neurophysiology)

We quantified the effect of perturbations on the activity of a flexor and an extensor muscle, the FCR (Flexor Carpi Radialis), and the ECU (Extensor Carpi Ulnaris). Surface EMG was recorded using a 16-channel MR-compatible bipolar amplifier (ExG, Brain Products, Munich, Germany) (Fig 2.2).

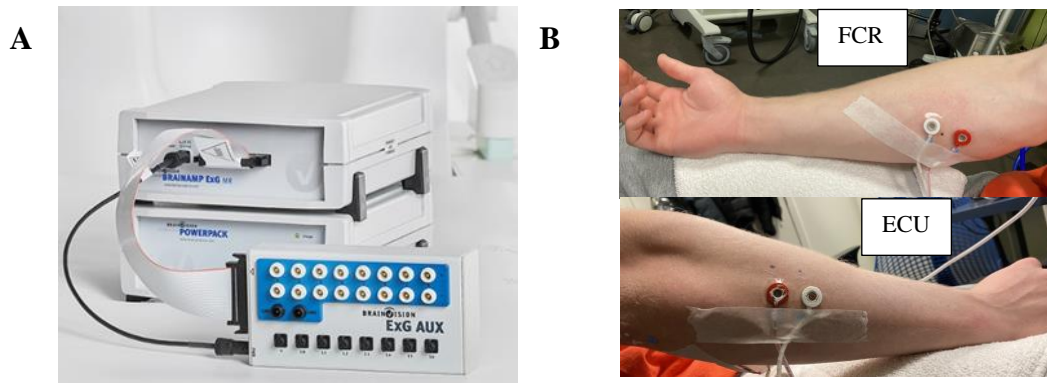


Figure 2.2 A) BrainAmp EXG-MR amplifier. B) Placement of EMG electrodes on the forearm muscles.

Following the same procedures used in previous work [60], after cleaning the muscle's skin with a 70% Isopropyl Alcohol solution, we located bipolar electrodes on the prominence of the muscle, parallel to the muscle fiber, and then used an abrasive Electrolyte-Gel to fill the central hole of each electrode, making sure that the contact impedance was lower than 10 k $\Omega$ . An electrode was also placed on the olecranon bone of the elbow joint as the grounding reference. Although this grounding electrode helped a lot with reducing the signal noise, we observed large noise in the EMG signal, especially from the ECU muscle, which was solved with applying a notch filter of 60Hz to the BrainVision amplifier software. Moreover, as our method included several pieces of equipment, we had several coiled and crossed cables around the EMG amplifier, which were one source of the observed noise as we observed a clearer signal when we uncoiled and separated the cables from each other. Additionally, avoiding proximity of the EMG amplifier to the power outlets was another solution that contributed to noise

reduction. In some subjects, placing the grounding electrode on other joints like ankle, was also helpful to reduce the noise (Fig 2.3).

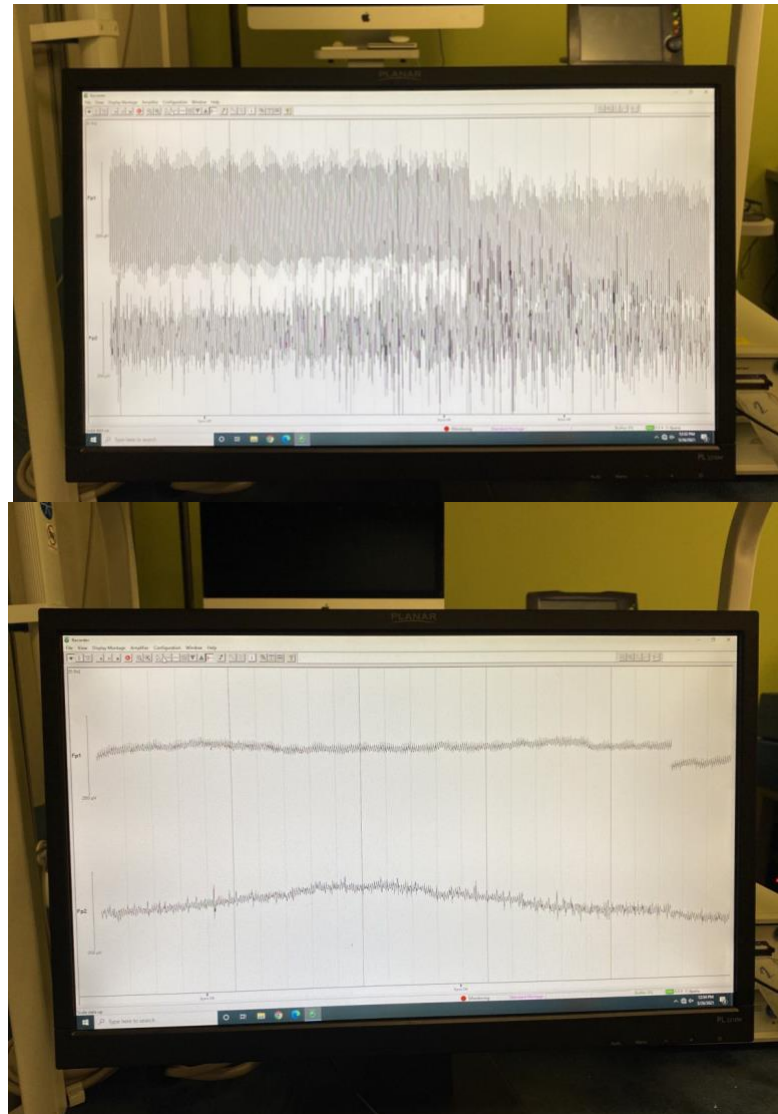


Figure 2.3 Screenshots indicating two EMG recordings from the same subject during the same session. (Top), signal with large noise at the beginning of the acquisition session. (Bottom), signal with reduced noise obtained after applying the notch filter and uncoiling the cables. Both EMG recordings are on the scale of  $200 \mu\text{V}$ , with signal from the FCR muscle on the top and signal from the ECU muscle on the bottom half of the screen.

### 2.3 Cortical TMS (neuromodulation)

A novel MR compatible TMS stimulation system has been used (Fig. 2.4). The system is composed of 1) a stimulator (MagPro X100 with MagOption), 2) an MCF-B65 Butterfly Coil and 3) an image-based navigation system that uses reflective markers and camera to enable localization of the coil over the stimulation region. This equipment also includes an MRI-compatible coil (MRI-B91) and camera for the inside the MRI scanner studies. 4) Localite TMS Navigator software 3.3.6.



Figure 2.4 A) The MagPro X100 with MagOption stimulator B) The MCF-B65 Butterfly Coil, C) an image-based navigation system that includes reflective markers placed on the subject's forehead and a camera to enable localization of the coil over the stimulation region.

### **2.3.1 Navigation processing**

Operating the TMS system initiated with the navigation processing which included several steps. First, we collected a high resolution T1 structural scan (magnetization-prepared rapid acquisition with gradient echo (MPRAGE): 0.7x0.7x0.7 mm<sup>3</sup> resolution, with TR=2600ms, and TE=4.64 ms; 256 slices with a 288x288 px per image, for a 256x288x288 mm<sup>3</sup> image volume) of the subject's brain, which was acquired through the Siemens 3T Prisma MR scanner located at the University of Delaware, Center for Biomedical and Brain Imaging (the report for the T1 structural scan's details is available in Appendix A). Thereafter, the scan was uploaded through the Localite TMS Navigator software 3.3.6, followed by the 'Brain Segmentation' process. During the brain segmentation, the Localite software performed the skull stripping and extraction of the brain tissue from the surrounding regions occurred. After that, two points were set on the scan, as the 'Target' and 'Entry' points. The 'Target' is determined as the point where we aimed to stimulate, and the 'Entry' is also determined as the point where we aimed to localize the coil on the skull. For this study, the 'Target' point was set in the motor cortex area, attributed to the forearm muscles, known as 'Motor Hot Spot' for these muscles. The 'Entry' point was the point aligned to the 'Target' point with a ~45° angle from the mid-sagittal line, which is optimal for TMS protocols of the cortex (Fig. 2.5) [91], [92].

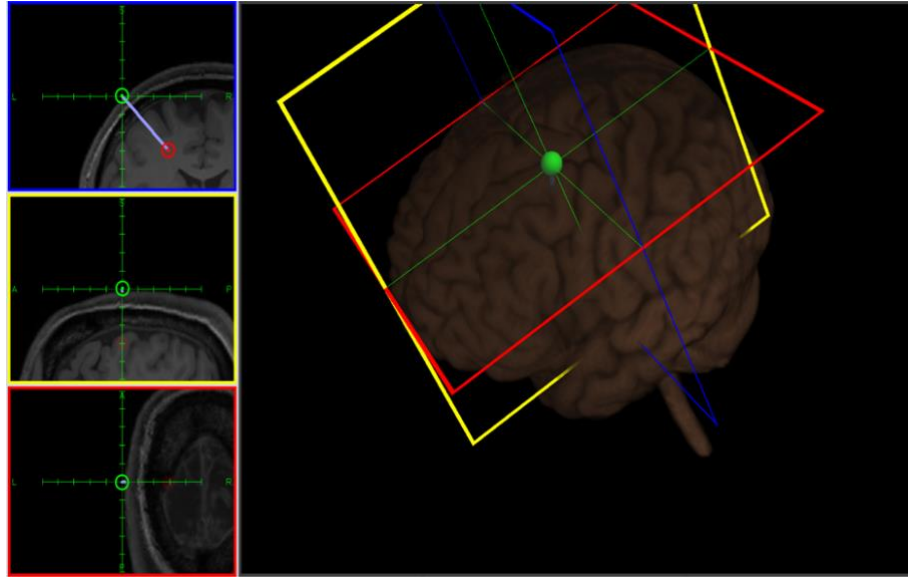


Figure 2.5 'Entry' (green) and 'Target' (red) points were set during the navigation processing as a guidance to localize the coil on the motor hot spot for forearm muscles.

This step was followed by 'Talairach definition', through which we defined three main cortical connector areas between the two brain hemispheres, including the 'Anterior commissure', 'Posterior commissure', and 'cortical Falx point' (Fig. 2.6).

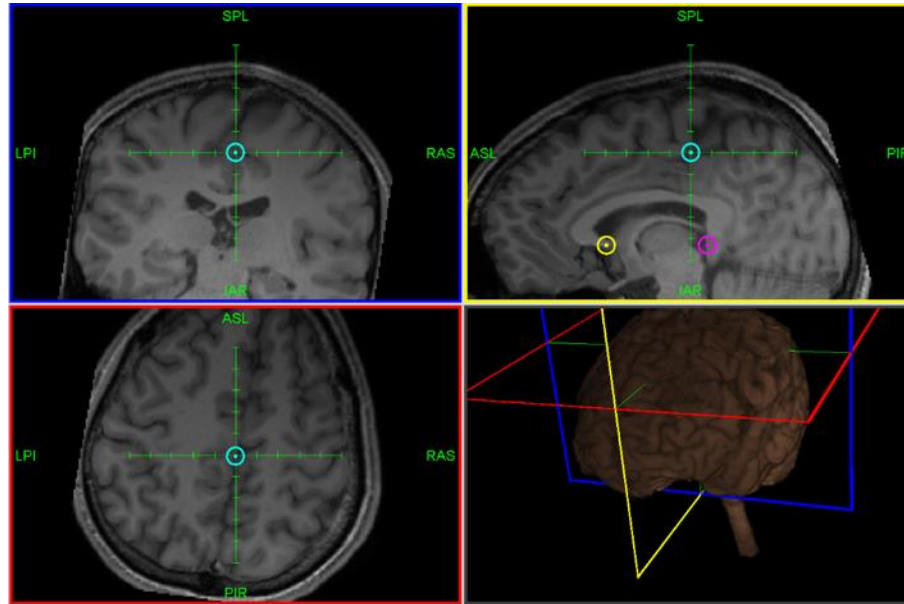


Figure 2.6 ‘Anterior commissure’ (yellow), ‘Posterior commissure’ (Pink) , and ‘cortical Falx point’ (blue) regions were set as the three main cortical connector areas between the two brain hemispheres.

‘Subject Registration’ was the last step of this navigation process, which included ‘landmark’ and ‘surface’ registrations. In the ‘landmark registration’ step, we defined three points of ‘Right Tragus’, ‘Left Tragus’, and ‘Nasion’ areas, in order to navigate the system with, and register the spatial area of the subject’s skull. After determining these points on the scan, we used a pointer to localize these regions on the subjects’ face, along with a headband attached to the forehead of the subject. Both of these pieces contained reflective markers, detected by the camera in front of the subject. This step was followed by the ‘surface’ registration, which was processed by moving the pointer side to side, front to the back, on the skull surface of the subject, until

covering the whole skull surface and reaching at least 200 points based on the navigator software counter (Fig. 2.7). This registration process is detailed in a tutorial video recorded from the MagVenture’s team training sessions, in the HuRo Lab shared drive (FSergi-001/Lab resources/Lab tutorials/TMS training session/AfternoonSession.mp4- from 1h:39min-1h:49min).

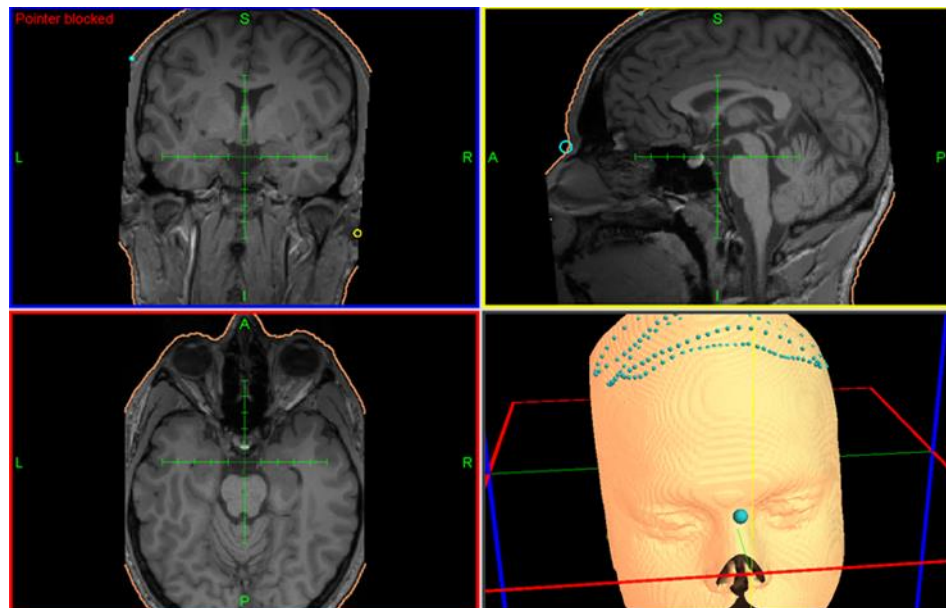


Figure 2.7 The pointer was driven side to side on the subject’s skull surface, indicated by the blue dots on the figure.

### 2.3.2 Stimulation processing

The stimulation processing started by switching to the ‘Stimulation’ mode in the same Localite TMS Navigator software 3.3.6. Based on the determined ‘Entry’ point and the aligned line to the ‘Target’ point in the navigation processing, an ‘Instrument marker’ was set in order to positioning the coil over the participant’s head oriented  $\sim 45^\circ$

from the mid-sagittal line. Subject head was also fixed with a chair-mounted brace to avoid having to adjust coil location during the experiments (Fig 2.8).

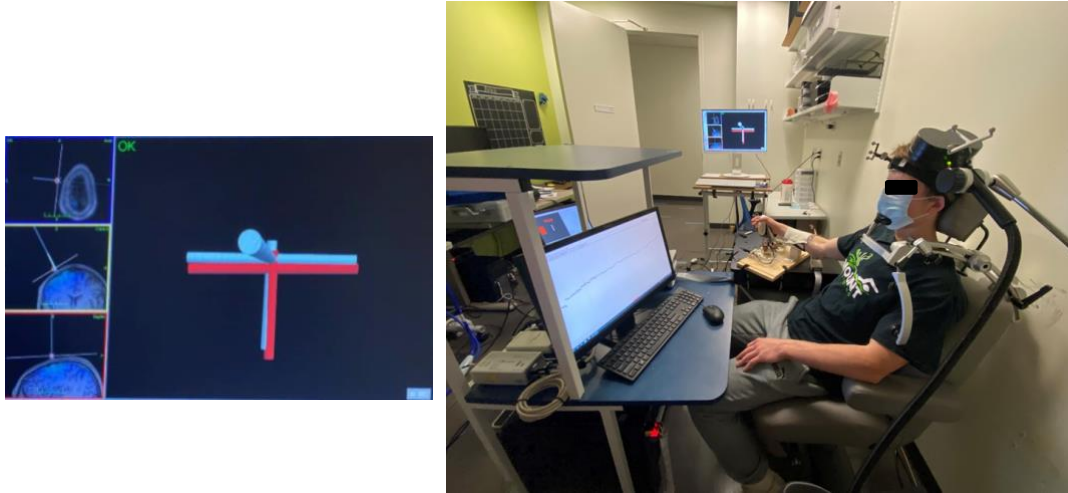


Figure 2.8 The butterfly coil was located on the left (contralateral) motor cortex of the subject, guided by the ‘Entry’ and ‘Target’ points, were set in the navigation processing.

#### **2.4 Determining the “cortical” motor threshold**

As the initial step, through a pilot study of 7 subjects, we measured Resting Motor Threshold (RMT) which is determined when the target muscle is at resting condition [67]. Thereafter, Active MT (AMT) was also measured. The AMT is typically determined during the condition when the target muscle is in a slight tonic contraction with an approximately 20% of the maximal muscle strength [62], [67]. The AMT indicates closely the threshold for inducing descending neural drive in the corticospinal tract’s fast-conducting neurons, which is justifiable as the initial recruited descending volleys can effectively discharge those spinal motoneurons with an approximate firing threshold in an active condition [62], [67].

To determine RMT, stimulus intensity was gradually increased from 20% MSO, in steps of 5% MSO until TMS consistently evokes MEPs with peak-to-peak amplitudes of  $>50 \mu\text{V}$  [67] in more than 5 out of 10 trials with an inter-stimulus time interval of 5 s. After that, stimulus intensity was gradually decreased in steps of 1% MSO until there are at least 5 positive responses out of 10 trials. This stimulus intensity was then defined as RMT. This measurement was based on the visual observation when the BrainVision Recorder screen was set on  $50 \mu\text{V}$  threshold for each muscle channel, and the MEPs which exceeded this threshold limits (either negative or positive) was considered as valid MEPs.

To determine AMT, instead, the threshold for the classification of an MEP was set to  $200 \mu\text{V}$ . Classifying an MEP during active contractions required extra care compared to RMT, since TMS interferes with the subject's ability to maintain a constant muscle contraction with a stable muscle background EMG activity of 10–20% of maximal voluntary contraction [62], [67], [84], [93]. In this regard, we instructed subjects to apply 0.3 Nm background muscle activity, cued by a screen in front of them displaying information collected via the F/T sensor embedded in the MR-StretchWrist. The MEPs were distinguished from the background muscle activity as they followed the TMS pulse application which could be detected both visually and via the MATLAB analysis by considering the TMS application timepoint in the analysis. Notably, the MEP induced during the AMT measurement was followed by a silent period (SP) on the EMG signal (Fig 2.9).

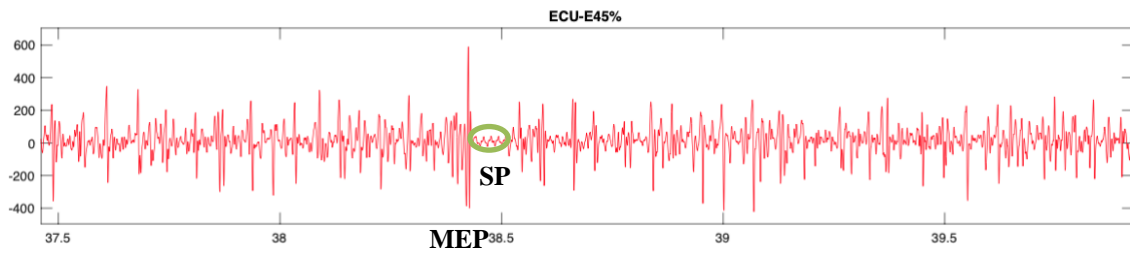


Figure 2.9 MEP evoked during AMT measurement from ECU muscle with a signal intensity of 45% MSO, which was followed by a SP on the EMG signal.

## 2.5 Synchronization of robotic perturbations, TMS, and EMG

Synchronization between robotic perturbations and TMS has been achieved by setting the TMS signal mode in ‘Twin’, waveform in ‘Biphasic’, and Timing control in ‘External Sequence control’ conditions. We used the biphasic TMS waveform, as this waveform was the only option in the stimulator settings to synchronize the TMS triggers with the EMG amplifier and the only possible waveform to be applied during the MR scanning for our future TMS-fMRI study. Through this setting, an analog voltage signal has been sent to the Trigger-IN port of the TMS amplifier using a real-time Quanser model running on a Q2-USB DAQ at 1 kHz sample frequency. The same DAQ was used to send commands to the robot triggering the perturbations. The Simulink model which was used to generate the abovementioned signals to the TMS amplifier and the robot from the Q2-USB DAQ is shown in Fig 2.10. This model is named as ‘MRSWControlNoMRIModelTMS\_REGULAR’ and is available here: FSergi-001\StudentFolders\Paria\Shareable\Paria Stim\StretchWristSoftware.



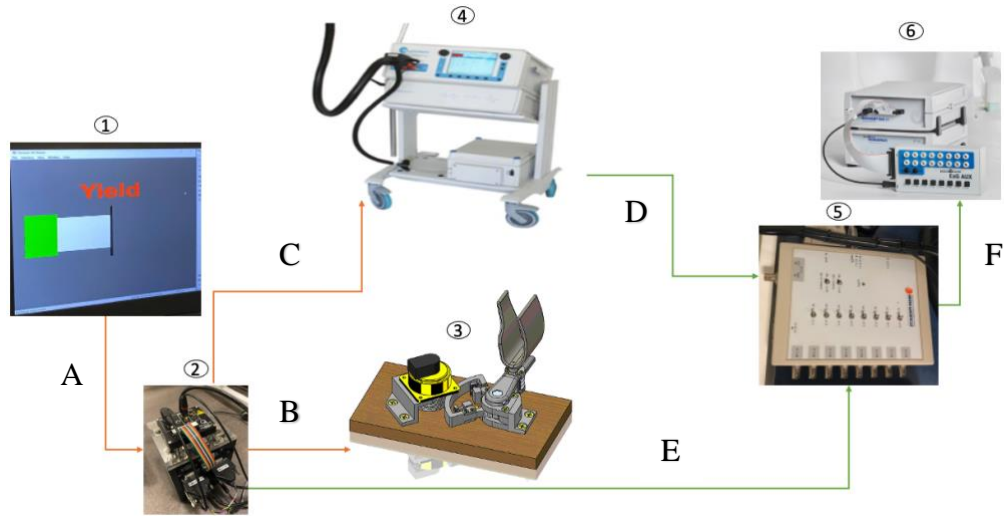


Figure 2.11 The synchronized Robot-TMS-EMG system. A Simulink model was ran on a laptop (1) mounted in front of the subject, cuing the background torque target, when the target was met, the control box (2), generates the trigger cued by the logic of the Simulink model and commands the motor of the MR-StretchWrist (3). The robot (3) implements a perturbation as controlled by the driver in the control box. The control box also sent triggers to the TMS stimulator (4) via the connection between the Trigger-In cable of the TMS stimulator and the Q2-USB DAQ on the control box (cable C), which resulted in discharge of the TMS stimulator. In order to synchronize the TMS and perturbations with the EMG recording, both the TMS stimulator and the control box sent triggers to the BrainVision system trigger box (5) (via Channel 15 and 7, respectively). The TMS trigger was sent via the Trigger-Out cable (D) and the perturbation trigger was sent via the cable connected to the Trigger-2 port of the control box (E). The BrainVision system trigger box then transferred both these triggers to the EMG amplifier (6) via the cable F, connecting the trigger box to the BrainVision system case, while recording the EMG signal from forearm muscles.

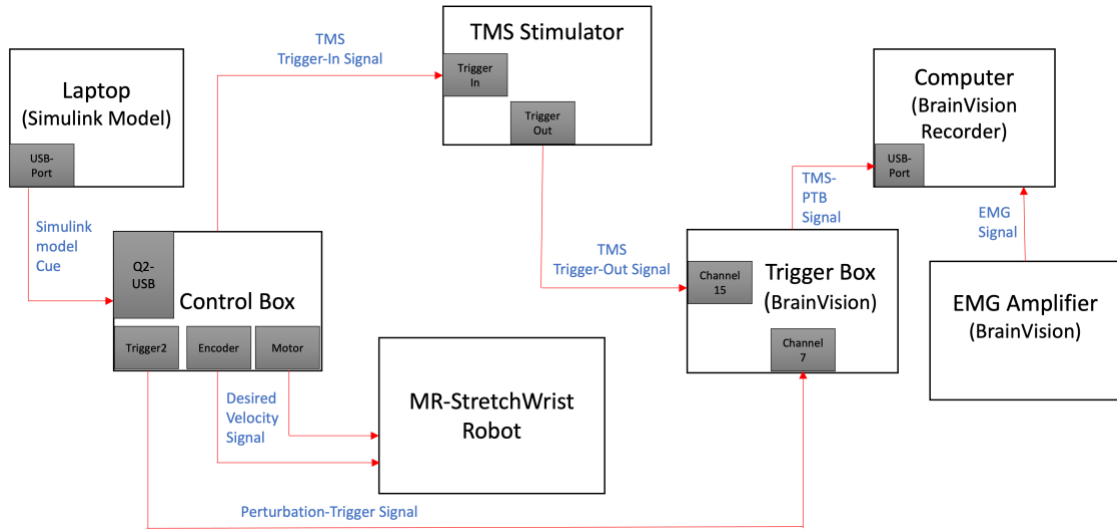


Figure 2.12 The functional diagram of the synchronized Robot-TMS-EMG system. Different components and the transmitted signals are shown.

To achieve inhibition of the supraspinal components of LLRs across multiple participants, it was important to manipulate the latency between perturbation onset and a motor-evoked potential (MEP), measured via surface EMG, a latency labeled  $T_L$  hereafter. To manipulate  $T_L$ , after measuring the AMT of each muscle through a simultaneous analysis during the experiment, we measured the latency between a TMS pulse and an MEP of the determined AMT, for each individual pulses delivered 5 s apart, which was calculated based on the difference on the EMG time points between the time TMS triggers were received and the time of evoked MEPs peaks, and then measured the average delay between the 10 trials, as  $T_1$  (the script used for this analysis is available here: [FSergi-001/StudentFolders/Paria/Shareable/AMT-T1](#)). Then, to achieve MEP latency of  $T_L$  relative to the perturbation onset, we applied a TMS pulse at time  $\Delta T = T_L - T_1$  (Fig. 2.13).

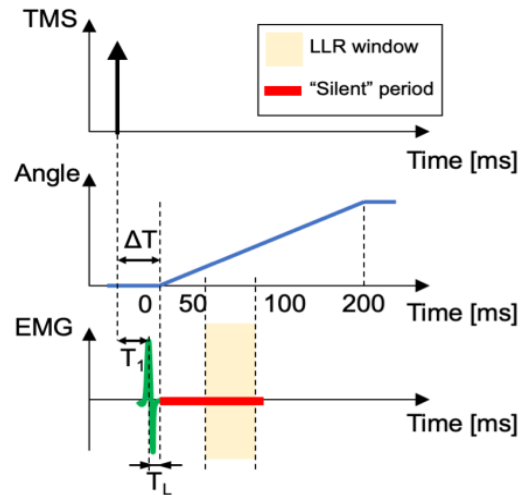


Figure 2.13 Timing diagram of the TMS pulse, the robotic perturbation, and MEP evoked on the active muscle.  $T_1$  is the latency between TMS and MEP,  $T_L$  is the desired MEP latency (relative to perturbation onset), and  $\Delta T$  is the delay to achieve a desired  $T_L$ . Following the MEP, there is a silent window of reduced motoneuron excitability, which we expected to result in a decrease of LLRa measured in response to perturbations.

It is known that different values of  $\Delta T$  will result in different inhibitory effects on LLR amplitude. The purpose of the application of TMS is to induce a silent period, which immediately follows the applied pulse, and lasts for roughly 150 ms [94], [95]. Current evidence on silent periods points to the fact that the inhibitory action measured in the first 50- 80 ms after an MEP is due to inhibition of predominantly spinal circuits. Instead, the inhibitory effect resulting more than 50 ms after the MEP is primarily due to inhibition of cortical circuits, and specifically intracortical inhibition [94].

As such, because TMS is used in this work to generate inhibitory action on the cortical input to motoneurons that produce the LLR, and compare it with the spinal

inhibitory effects, we tested three values of parameter  $\Delta T$ , including the  $T_1$  (which induced MEPs evoked at the same time as the perturbations started),  $T_1+20\text{ms}$ , and  $T_1+50\text{ms}$ . With these delay conditions, we expect the  $T_1$  delay condition to demonstrate inhibition of both spinal and supraspinal circuits during the time window corresponding to an LLR, while the other two delays were expected to inhibit more specifically supraspinal circuits around the time window considered for LLRs (50 ms - 100ms from perturbation onset). As an example, to achieve MEP arrival 20 ms before perturbation onset, for a  $T_1$  latency of 35 ms, we would apply a TMS pulse  $\Delta T=55$  ms before perturbation onset. In these conditions, the silent period would last through the entire LLR window, inhibiting spinal circuits during the short-latency phase, and inhibiting supraspinal circuits during the LLR phase, as desired.

### **2.5.1 Example of synchronized robot-EMG-TMS**

The plots below (Fig. 2.14) demonstrate our synchronized method result on how the TMS pulse with a time delay ( $T_L$ ) of 20ms and  $T_1$  of 35ms has been synchronized with the robotic perturbations and EMG activity recording from the FCR muscle. Also, another plot from the conditions without TMS application, for the same subject and experiment, is illustrated.

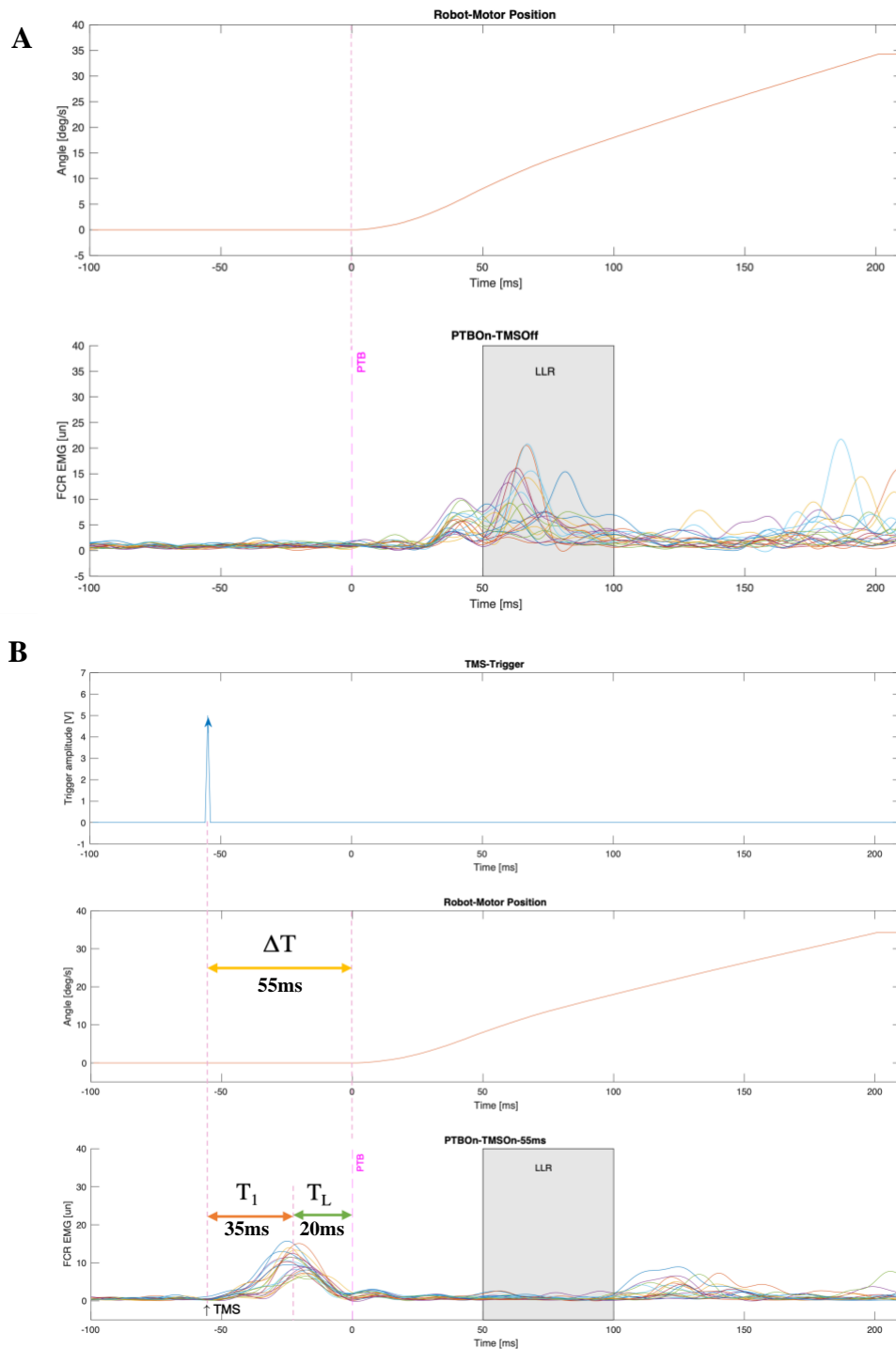


Figure 2.14 A) The motor-position and the normalized EMG activity recorded from the FCR muscle in conditions without a TMS pulse. The shaded area shows the evoked LLR activity window. B) The applied TMS trigger, the motor-position and the normalized EMG activity recorded from the FCR muscle for the same subject, when the TMS pulse was applied with 55ms delay ( $T_1$  (35) +  $T_L$  (20) =  $\Delta T$  = 55ms) to the robot perturbation. The shaded area shows the inhibited LLR activity window.

## Chapter 3

### QUANTIFYING THE INHIBITORY EFFECT OF SUBTHRESHOLD TMS ON THE CORTICAL CONTRIBUTION TO LLRs MEASURED IN THE FOREARM MUSCLES

Using the synchronized method described in the previous chapter, we quantified the inhibitory effect of subthreshold TMS on the cortical contribution to LLRs measured in the forearm muscles, in two groups of healthy participants, considering two levels of stimulation intensity, and three different time delays between the application of TMS and the velocity-controlled perturbation onset. The study design and results are detailed in the sections below.

#### 3.1 Materials and methods

##### 3.1.1. Participants and study design

This study was designed to evaluate the effects of subthreshold TMS applied to the primary motor cortex on the amplitude of long-latency responses elicited by robotic perturbations, with the ultimate goal of identifying the combination of TMS stimulation parameters that would maximally inhibit the supraspinal contribution to LLRs. To this purpose, we exposed two groups of healthy participants to two TMS intensities (between-subject factor, 90% and 95% of their active motor threshold – AMT). TMS was applied to all participants with three different time delays, with levels  $T_1$  (which induced MEPs at the same time as the robot perturbations started),  $T_2$  ( $T_1+20\text{ms}$ , where an MEP would be induced 20 ms sooner than the perturbation onset), and  $T_3$  ( $T_1+50\text{ms}$ ). This study quantified, the effect of TMS parameters on the amplitude of LLRs recorded through surface EMG signals from FCR muscle, which was stretched through the wrist extension perturbations (velocity: 150 deg/s, duration: 200 ms). This experiment

included total of 100 randomized trials with five conditions, including three time delays (T<sub>1</sub>, T<sub>2</sub> and T<sub>3</sub>) conditions and two additional conditions of (TMS Off- Perturbation (Pert) off), and (TMS Off-Pert On).

### **3.1.1.1 Participants**

Fourteen healthy subjects (9 males, 5 females, age between 21-34 years) were included for this experiment with 6 subjects allocated to group 1 (90%AMT) and 8 subjects to group 2 (95%AMT). Inclusion criteria were: (i) between 18 and 50 years of age, (ii) right-hand dominance, defined by the Edinburgh handedness test 44 with outcome >48. Exclusion criteria were any neural or biomechanical impairment history in the upper extremities, history of neurological or psychiatric impairment, or any other contraindications to TMS, as taking the medications which lowered the seizure threshold. All subjects provided informed written consent prior to data collection. This study was approved by the Investigation Review Board of the University of Delaware Protocol no. 1545543-2 (the approval document is available in Appendix B) and was conducted in accordance with the Declaration of Helsinki.

### **3.1.2 Experimental procedures**

In all sessions, the participant was sitting in the experiment chair, with a chair-mounted brace fixing their head and the TMS coil was also located on their contralateral motor cortex. The subject's forearm was placed in the MR-StretchWrist robot. Surface EMG activity was recorded from his FCR muscle. To both reduce the complexity of the experimental protocol, and to increase the statistical power in quantifying the effects TMS parameter on muscle LLRs, we have selected to quantify sEMG from only the FCR muscle. FCR revealed clearer perturbation-related signal and robustness to noise

in preliminary developmental steps. Via a graphical interface developed in MATLAB/Simulink, the participant was cued to apply a background torque of 0.3 Nm of wrist flexion, measured via the F/T sensor embedded in the MR-StretchWrist (Mini27Ti, ATI Industrial Automation, Apex, NC). When the participant achieved a level of torque within 0.07 Nm of the 0.3 Nm (the target value), the bar in the interface changed color to green indicating success in achieving the cued contraction state (Fig 3.1).

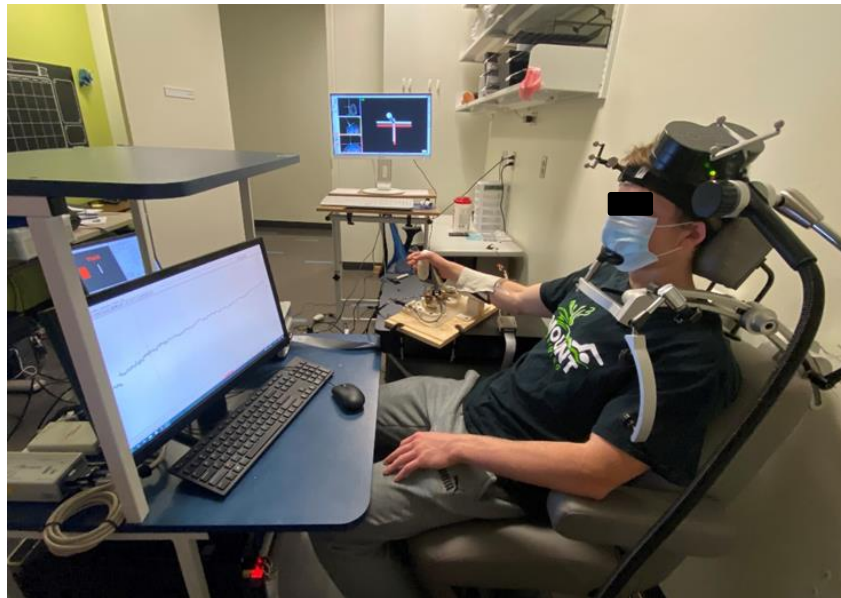


Figure 3.1 Subject seated on the chair with TMS coil placed on his left motor cortex and his right forearm placed in the hand support of robot, cued by a graphical interface on the laptop.

### 3.1.2.1 Subject specific measurements

As the initial step for this experiment, we measured the AMT and  $T_1$  delay attributed to this threshold, for each subject.

The TMS stimulation was started at 20% and increased by 10% to achieve the lowest intensity which induced at least 5 out of 10 trials with MEPs larger than 200  $\mu\text{V}$ , with inter-stimulus interval of 5 s, which was set on the BrainVision EMG recorder software. The participant was instructed to maintain the background torque when the TMS stimulation was delivered and rest his forearm between different intensity stimulations. A simultaneous signal analysis by MATLAB, was performed in order to quantify the MEPs (larger than 200  $\mu\text{V}$ ) counts for different intensities (the intensities we observed that could evoke large MEPs) and also calculate  $T_1$  for the AMT intensity, which was indicated as the averaged time delay between the MEP peaks and time of TMS pulses application (the script used for this analysis is available here: FSergi-001\StudentFolders\Paria\Shareable\AMT-T1).

### **3.1.2.2 Perturbation Experiment**

We conducted experiments on two groups of right-handed healthy subjects with two intensity levels of 90% MSO for group 1 ( $n=6$ , with two repetitions for two of the subjects), and 95% MSO for group 2 ( $n=7$ ). For each group, the biphasic TMS pulses were randomly delivered over the left motor cortex, with three different  $\Delta T$  latency levels equals to  $T_1$ ,  $T_1+20\text{ms}$ , and  $T_1+50\text{ms}$ . LLRs were recorded through surface EMG signals from the FCR muscle, which was stretched through the constant velocity ramp-and-hold extension perturbation (velocity: 150 deg/s) applied to the wrist joint. Each condition was repeated 20 times with random sequence. Forty additional control trials in two conditions of (TMS Off- Pert off), and (TMS Off-Pert On) were also randomly applied to control for fluctuations in the signal arising from background muscle activity, and to establish the LLRa in the absence of TMS pulses, respectively. Before each perturbation, participants were cued to generate a background torque of 0.3

Nm in wrist flexion via the graphical user interface, and to maintain this background torque until the end of perturbation (Do not intervene condition). They were asked to relax their muscles when the robot initiated to return as the perturbation was ended.

### 3.1.3 Data analysis

Processing of the raw EMG data was conducted using MATLAB code with the similar filtering approach we used in our previous work [59]. This processing was based on a standard pipeline including three steps of a band-pass filtering to remove high-frequency noise and motion artifacts (4th order Butterworth filter with cut-off frequencies 20 Hz and 250 kHz), followed by a signal rectification, and then a low-pass filtering to extract the EMG signal's envelope (4th order filter with cut-off frequency of 60 Hz). Prior to digitization, a 60 Hz notch filter was also enabled in the BrainVision EMG recorder settings to reduce the signal noise. To extract the magnitude of the long-latency response specific to each perturbation, the average signal intensity in the LLR window ([50 100] ms after perturbation onset was calculated. All EMG measures were divided by the average intensity of the rectified signal measured during background within the 100-50ms before the perturbation onset (130-80ms before perturbation for T<sub>3</sub> to make sure we avoid signal fluctuations due to the TMS effect), to allow between-participant comparisons. To estimate the percentage reduction in the LLRa in each condition in comparison to the TMS Off- Pert On condition, we normalized the data based on the subtraction of the averaged LLRa for each trial per each condition from the total averaged LLRa of the TMS Off- Pert On condition, which result then was also divided by the total averaged LLRa of the TMS Off- Pert On condition:

$$\text{NormLLRa} = \frac{[(\text{LLRa for trial}) - (\text{Avg LLRa, TMS Off} - \text{Pert On})]}{(\text{Avg LLRa, TMS Off} - \text{Pert On})}$$

### 3.1.4 Statistical analysis

JMP Pro 15 version software was used for the statistical analysis. Statistical analyses were conducted to identify a combination of pulse amplitude and timing that reduced LLRa compared to the TMS Off- Pert On condition. The outlier data were removed from the group-level and repeatability analyses to increase the accuracy, using screening for outliers with Huber method (data were organized “by participant” so separate outlier identification and exclusions were conducted for each participant), which resulted in extracting 28 outliers from all data in both groups and 13 outliers from subject 6 data in the repeatability analysis. These datapoints were removed before normalizing the LLRa and applying the statistical model on the remaining datapoints.

#### 3.1.4.1 Group-level analysis

Group-level analysis was performed using a linear mixed model with fixed factors: 1) Stimulation mode – categorical variable with 5 levels: i) TMS Off, Pert Off, ii) TMS Off, Pert On, iii) TMS On (T<sub>1</sub>), Pert On, iv) TMS On (T<sub>2</sub>), Pert On and v) TMS On (T<sub>3</sub>), Pert On, with three T<sub>L</sub> levels of 0, 20 and 50 ms, referred to as T<sub>1</sub>, T<sub>2</sub> and T<sub>3</sub>, respectively, all measured during a perturbation) and 2) TMS intensity – categorical variable with 2 levels (90% AMT and 95% AMT), and random factor “subject”. The model was used to explain the variance in the outcome measure LLRa as:

$$\text{LLRa} = a_0 + a_1 \text{ TMS mode} + a_2 \text{ TMS intensity} + a_3 \text{ TMS mode} * \text{ TMS intensity} + a_{\text{Subject}(i)},$$

After establishing the significant effect of the ‘TMS mode’ factor and no significant effect of ‘TMS intensity’ and the ‘TMS mode\*TMS intensity’ interaction, we divided the mixed model by the group (TMS intensity) and applied separate mixed model with ‘TMS mode’ as the fixed factor and ‘subject’ as the random effect, for each

group. These analyses were followed by the Dunnett's test to perform post-hoc tests while controlling for the false-positive rate associated with the multiple comparisons, using the TMS Off, Pert On condition of each group, separately, as control conditions.

#### **3.1.4.2 Subject-specific analysis**

The Shapiro-Wilk test was used to check the normal distribution of the data. Because individual participant data were not normally distributed, in subject-level analysis, the Wilcoxon/Kruskal-Wallis [96] test to quantify how stimulation mode modulated the LLRa, separately, for each participant. Thereafter, the Steel method [97] was used as the nonparametric comparison test with a control group, which was the subject-specific measurements obtained in the TMS Off, Pert On condition. Due to the four post-hoc tests performed per group (comparisons to control condition), we used a Bonferroni-corrected alfa level of  $0.05/4=0.0125$  to control for multiple comparisons.

#### **3.1.4.3 Repeatability analysis**

Two of the subjects (subjects 1 and 6 from group1) were tested two times to check for the repeatability of the results and individual-level variance. A full factorial least square means model was used to evaluate the effects of the 'Day', 'Condition', and their interaction on the LLRa.

#### **3.1.5 Power analysis**

Based on the effect size calculated from the previous works [82], [98], a sample of  $N=12$  participants was sufficiently powered to detect a significant effect at the conventional type-I error rate ( $\alpha=0.05$ ), with desired statistical power ( $\beta=0.9$ ). Considering an attrition rate of 20%, we recruited a larger number of participants ( $N=14$ ) which allowed interim adjustments to our protocol, as it was customary for a

methods development aim. One subject was excluded as the desired MEPs for measuring their AMTs were not observed during the subject-specific measurement step of the experiment.

## **3.2 Results**

### **3.2.1 Subject specific measurements results**

Fourteen healthy subjects (9 males, 5 females, aged between 21-34 years) were allocated in two groups. One subject did not induce MEPs with the desired amount and amplitude to measure the AMT, although the coil was moved for 1 cm in the surrounding area of the target point and the subject registration was repeated. The Localite software also did not detect the coil properly for this subject, although it was accurately touching the skull on the entry point and the signal line was aligned with the entry and target points.

TMS intensity of 90% MSO was used for group 1 (n=6)- with two repetitions for two of the subjects to check for the individual-level variance. Their first experiment data is shown in this section (table 3.1), which was also used in the group-level analysis, and the intensity of 95% MSO was used for group 2 (n=7). AMT and  $T_1$  (the averaged time delay between application of the TMS pulses and peaks of MEPs attributed to each subject's AMT intensity) were measured. AMT was ranged between 23-94% MSO, with a mean  $\pm$  SD of  $61.54 \pm 21.48\%$  MSO and  $T_1$  was ranged between 6-35ms with a mean  $\pm$  SD of  $28.15 \pm 7.15$ ms.

In group 1, AMT ranged between 49-80% of MSO (mean  $\pm$  SD:  $59.17 \pm 11.03$ ), and the applied stimulus intensity (90% of AMT) ranged between 44-72%MSO (mean  $\pm$  SD:  $53.33 \pm 9.91$ ).  $T_1$  for this group ranged between 25-35 ms (mean  $\pm$  SD:  $30.33 \pm$

3.44). In group 2, AMT ranged between 23-94% of MSO (mean  $\pm$  SD: 63.57 $\pm$ 28.48), and the applied stimulus (95% of AMT) ranged between 22-89% of MSO (mean  $\pm$  SD: 60.43  $\pm$  26.95). T<sub>1</sub> for this group ranged between 6-33 ms (mean  $\pm$  SD: 26.29 $\pm$ 9.14). Table 3.1 illustrates all subjects' demographic data, AMT, T<sub>1</sub>, and the calculated (90 or 95%) of the AMT applied in the experiment.

Table 3-1 Demographic and subject-specific measurement data of all subjects

Group	Subject	Age	Sex	AMT (%MSO)	T <sub>1</sub> (ms)	%AMT (%MSO)
Group 1 90% AMT (n=6)	1	21	m	85	32	77
	2	24	m	49	32	44
	3	24	m	54	29	49
	4	23	f	62	35	56
	5	21	f	56	32	50
	6	28	m	54	24	49
Group 2 95% AMT (n=7)	7	28	m	23	6	22
	8	34	m	30	29	29
	9	28	f	74	27	70
	10	25	f	80	33	76
	11	32	m	90	29	86
	12	29	m	94	29	89
	13	22	f	54	31	51

AMT: Active Motor Threshold, MSO: Maximum Stimulator Output, m: male,  
f: female

### 3.2.2 Observations from selected participants

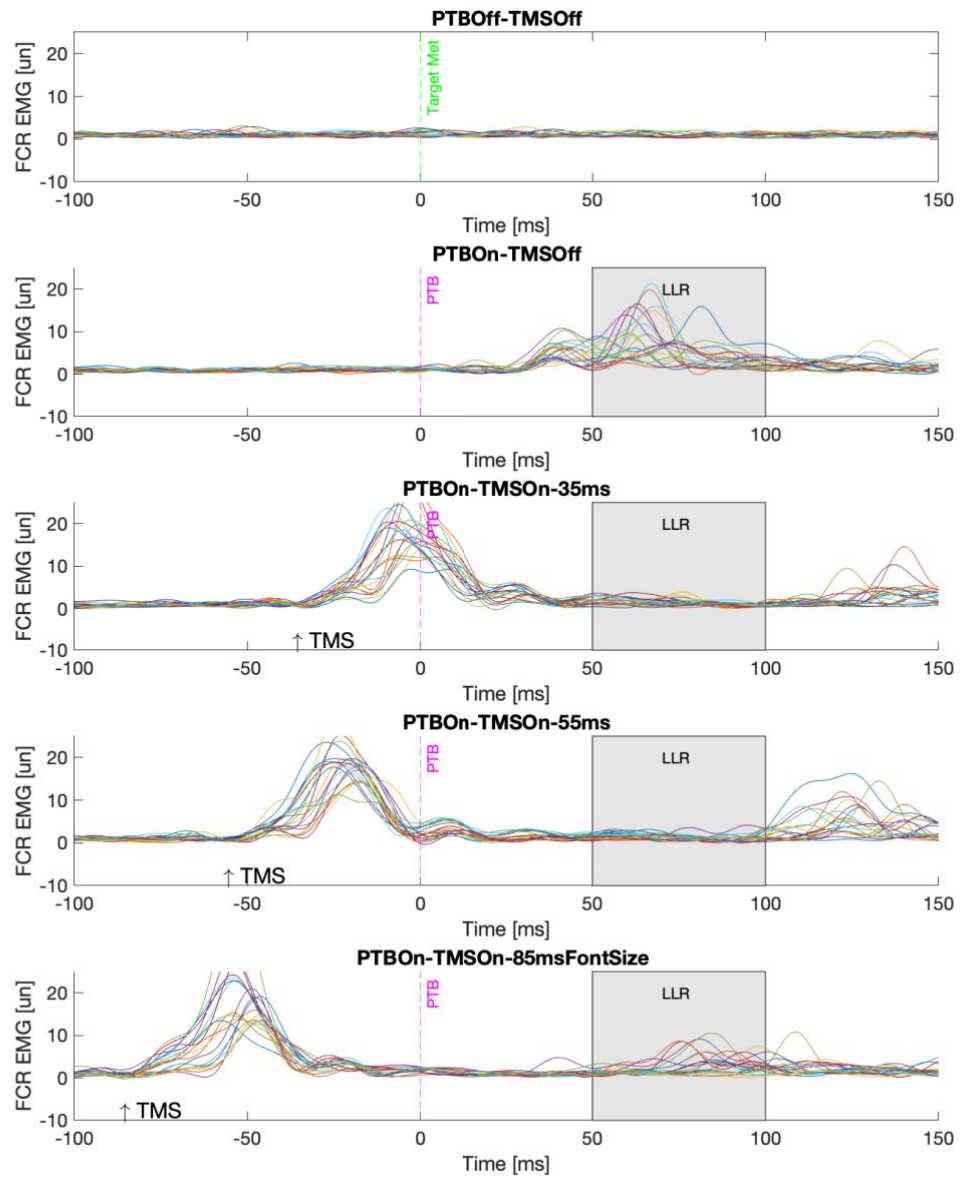
The signal analysis plots for one subject from each group are provided in Fig. 3.2 and Fig 3.3. Specifically, Fig 3.2A demonstrates the rectified EMG signal time series recorded from the FCR muscle of subject 4 from group 1, in all five study conditions, followed by the plots (Fig 3.2B) of the averaged  $\pm$  SD of the rectified EMG signal time series for the 20 trials in each experimental condition. This subject had an AMT of 62% MSO, and 90% AMT of 56% MSO, with a  $T_1$  of 35ms.

Steel method comparison revealed a significant reduction in LLRa for all three  $T_L$  latencies in comparison to the TMS Off-Pert On control condition, with p-value  $<0.0001$  for  $T_1$ , and  $T_2$  ( $T_1+20ms$ ) conditions, and p-value= 0.0001 for  $T_3$  ( $T_1+50ms$ ) condition.

Fig 3.3A demonstrated the rectified EMG signal time series recorded from the FCR muscle of subject 12 from group 2, in all five study conditions, followed by the plots (Fig 3.3B) of the averaged  $\pm$  SD of the rectified EMG signal time series for the 20 trials in each experimental condition. This subject had an AMT of 94% MSO, and 95% AMT of 89% MSO, with a  $T_1$  of 29ms.

Steel method comparison with the TMS Off-Pert On condition as the control group, for this subject also revealed reduction in LLRa for all three  $T_L$  latencies with p-value of 0.0252 for  $T_1$ , p-value of 0.0606  $T_2$  ( $T_1+20ms$ ) conditions, and p-value= 0.0397 for  $T_3$  ( $T_1+50ms$ ) condition.

A



B

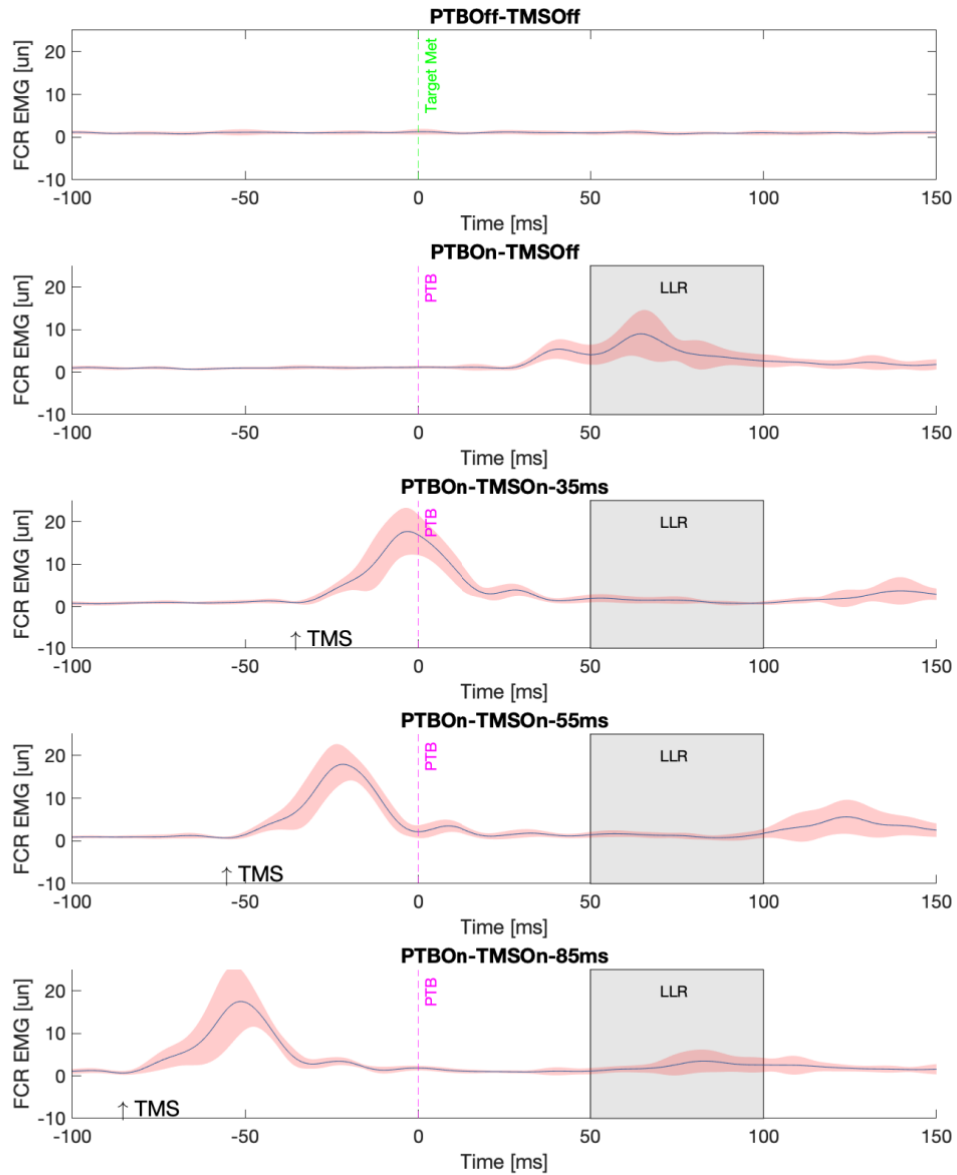
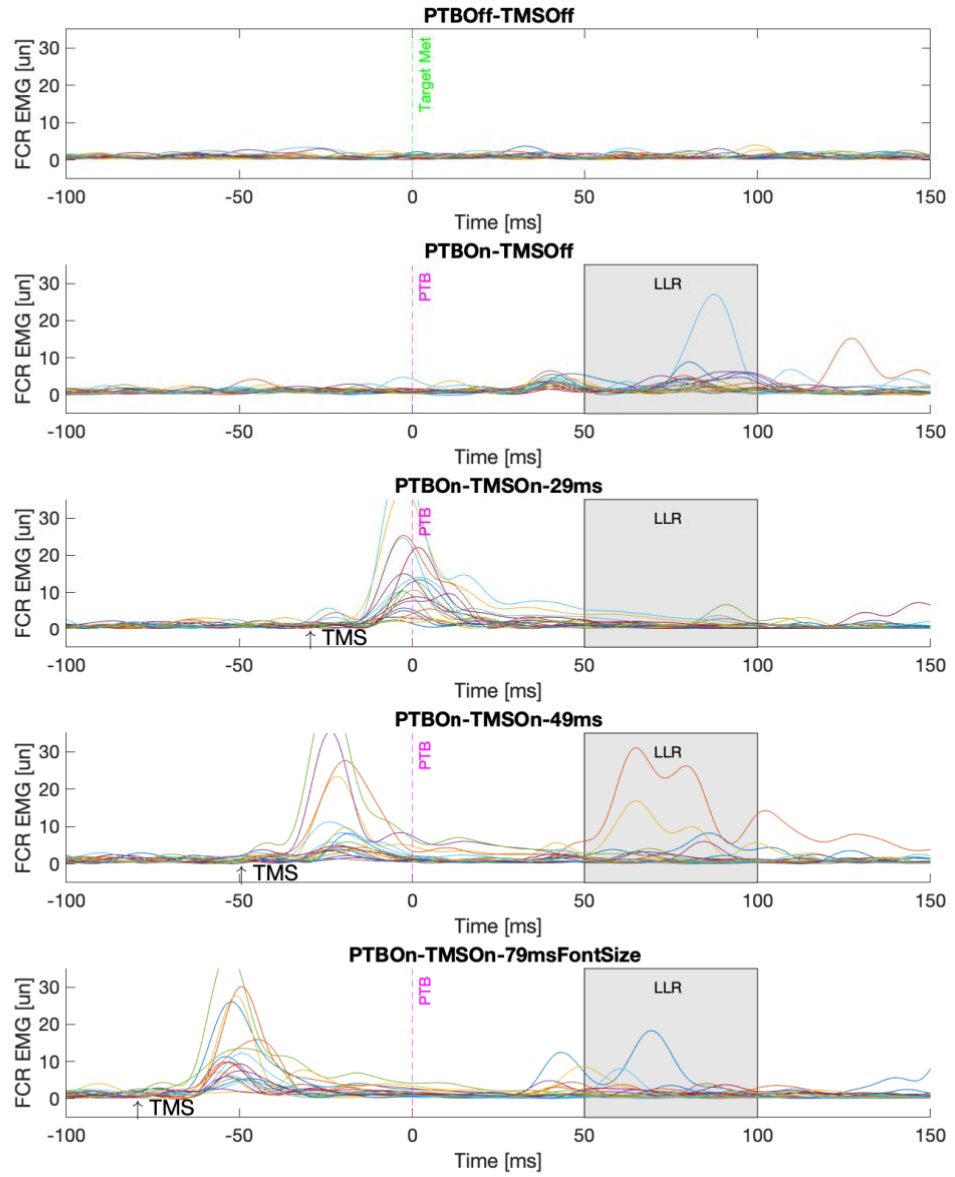


Figure 3.2 A) plots of all experimental conditions for one subject from group 1 (90%AMT). Rectified EMG signal recorded from the FCR muscle, for 20 trials per condition, is illustrated in each plot. The shaded area is the LLR activity on EMG signal between 50-100ms after the stretch onset. The area under the curve within this shaded area was used as the LLRa measurement. B) The same plots averaged  $\pm$  SD of the rectified EMG signals for the 20trials in each experimental condition is shown. The pink areas are attributed to the  $\pm$  SD.

A



B

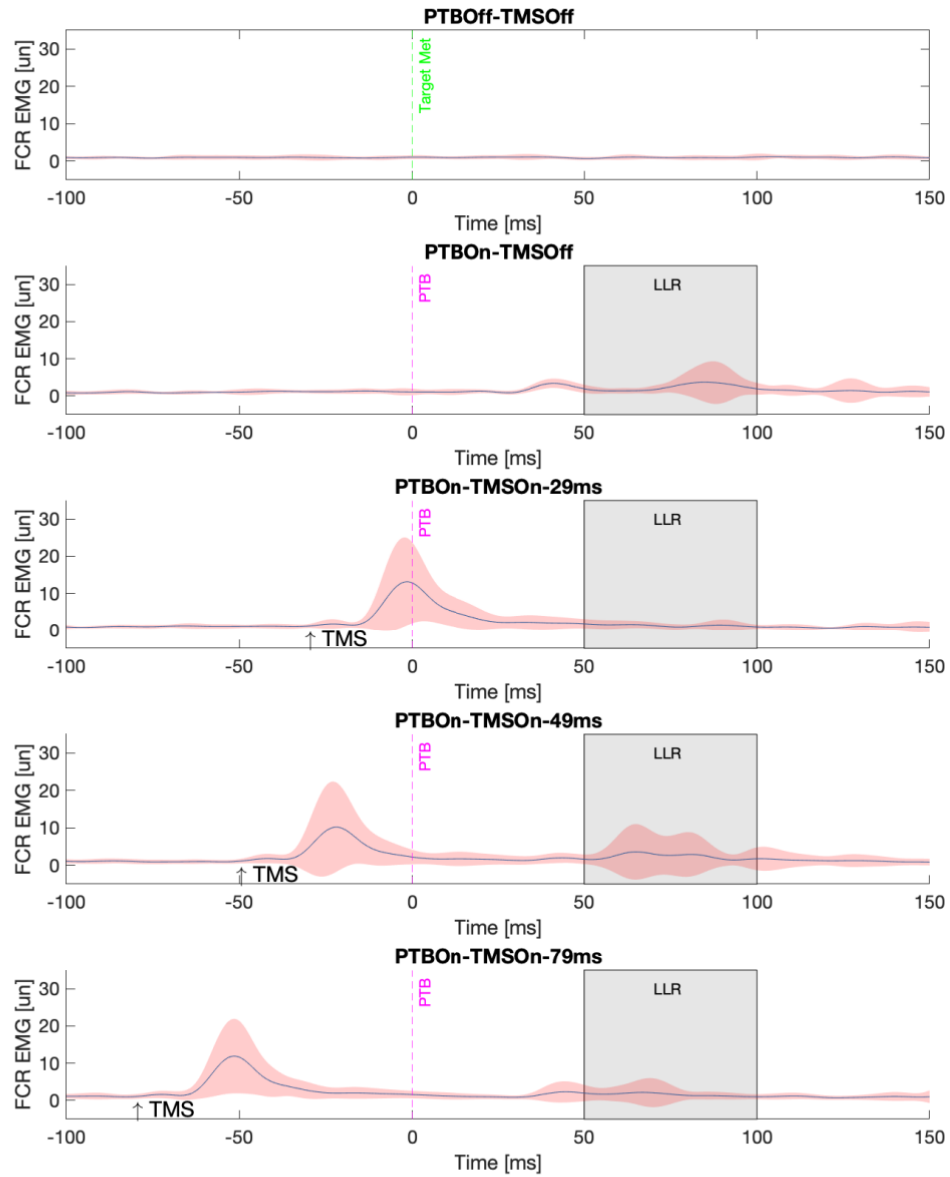


Figure 3.3 A) plots of all experimental conditions for one subject from group 2 (95%AMT). Rectified EMG signal recorded from the FCR muscle, for 20 trials per condition, is illustrated in each plot. The shaded area is the LLR activity on EMG signal between 50-100ms after the stretch onset. The area under the curve within this shaded area was used as the LLRa measurement. B) The same plots averaged  $\pm$  SD of the rectified EMG signals for the 20 trials in each experimental condition is shown. The pink areas are attributed to the  $\pm$  SD.

### 3.2.3 Group-level analysis

Mixed model analysis revealed that factor ‘condition’ significantly modulated the LLRa ( $p < 0.001$ ). However, the factor ‘group’ ( $p = 0.751$ ) and the interaction between factors ‘group’ and ‘condition’ ( $p = 0.097$ ) didn’t modulate the LLRa significantly.

Dunnett’s test sets upper and lower decision limits (UDL and LDL, respectively) based on the control value were used to perform post-hoc tests using the TMS Off, Pert On control condition. In all post-hoc tests, an inhibitory effect of TMS intensity at 90% AMT was established at all  $T_L$  latencies on the LLRa, with the  $T_1$  resulting in a 14.1% reduction that was not significant ( $p = 0.102$ ),  $T_2$  and  $T_3$  resulted in a significant reduction of 20.3% ( $p = 0.008$ ), and 22.8 % ( $p = 0.002$ ), respectively. Background muscle activity (TMS Off- Pert Off) condition was substantially lower than all other conditions, indicating the capability of eliciting LLRs via robotic perturbations both in presence and in absence of TMS. Dunnett’s test results are illustrated in Table 3.2.

Table 3-2 Dunnett’s test results with TMS Off- Pert On, group 1, control condition

Condition	Group	LLRa reduction (%)	Adjusted Lower 95%	Adjusted Upper 95%	Adjusted P-value
T1	1	-0.140794	-0.300845	0.019256	0.1022
T2	1	-0.202520	-0.362585	-0.042454	0.0076
T3	1	-0.227653	-0.387682	-0.067625	0.0021
T off-P off	1	-0.539132	-0.699152	-0.379112	<.001

Based on the Dunnett’s test post-hoc tests, a significant inhibitory effect of TMS intensity at 95%AMT was established at the T<sub>2</sub> latency on the LLRa, with 15.1 % reduction (p=0.017), as well as T<sub>3</sub> condition which resulted in the largest reduction in LLRa across both groups, equal to 25.3% (p<0.001), on the LLRa. However, T<sub>1</sub> resulted in non-significant 3.5% increase (p=0.912). Background muscle activity (TMS Off-Pert Off) condition was significantly lower than all other conditions. Dunnett’s test results are illustrated in Table 3.3.

Table 3-3 Dunnett’s test results with TMS Off- Pert On, group 2, control condition

<b>Condition</b>	<b>Group</b>	<b>LLRa reduction (%)</b>	<b>Adjusted Lower 95%</b>	<b>Adjusted Upper 95%</b>	<b>Adjusted P-value</b>
T1	2	0.034737	-0.094619	0.164094	0.9117
T2	2	-0.150966	-0.280786	-0.021145	0.0165
T3	2	-0.253056	-0.382168	-0.123945	<.001
T off-P off	2	-0.547737	-0.676621	-0.418854	<.001

The mixed model analysis also revealed a between group comparison, which demonstrated a significant different in the LLRa modulation for T<sub>1</sub> condition between the groups (p= 0.035); however, the LLRa reduction for T<sub>2</sub> and T<sub>3</sub> conditions were not significantly different between the two study groups (p=0.536 and p=0.760, respectively).

The results of the group-level analysis are summarized in Fig. 3.4, which includes the least square means of LLRa in comparison to each group’s TMS Off- Pert On condition with the significant modulations denoted by the asterisks, based on the Dunnett’s test results.

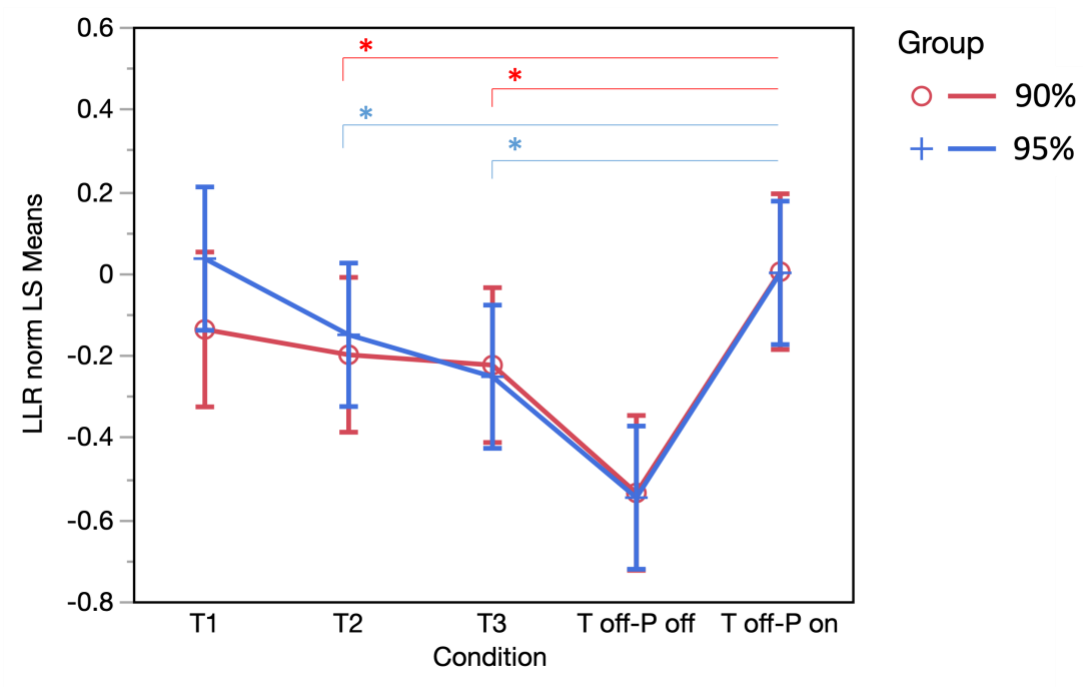


Figure 3.4 Least square means plots. Each group five experimental conditions compared by its TMS off-PerT On condition (bars indicate the standard errors). The asterisks denote the significant results based on the Dunnett’s test results.

**3.2.4 Subject-level analysis**

Via analysis of the subject-specific Wilcoxon/Kruskal-Wallis tests and post-hoc comparisons conducted via the Steel’s method, we established that a significant reduction in LLRa was measured in several conditions in both groups. Specifically, the T<sub>1</sub> condition significantly reduced LLRa in 2/6 participants exposed to the 90% AMT condition and in 1/7 participants exposed to the 95% AMT condition. The T<sub>2</sub> condition significantly reduced LLRa in 4/6 participants exposed to the 90% AMT condition and in 2/7 participants exposed to the 95% AMT condition. Moreover, the T<sub>3</sub> condition

significantly reduced LLRa in 5/6 participants exposed to the 90% AMT condition and in 3/7 participants exposed to the 95% AMT condition.

In group 1, for T<sub>1</sub> condition, the LLRa changes with a range of -0.870-10.413 (mean±SD = -0.199±1.031, median= -0.0481), for T<sub>2</sub> and T<sub>3</sub> conditions, the LLRa changes with a range of -0.880-2.746 (mean±SD = -0.355±0.586, median= -0.0588), and -0.890-6.646 (mean±SD= -0.347±0.754, median= -0.0577), respectively. In group 2, for T<sub>1</sub> condition, the LLRa changes with a range of -0.772-3.946 (mean±SD = 0.028±0.638, median= -0.0105), for T<sub>2</sub> and T<sub>3</sub> conditions, the LLRa changes with a range of -0.887-6.652 (mean±SD = -0.083±0.895, median= -0.0361), and -0.886-2.077 (mean±SD = -0.287±0.542 median= -0.491), respectively. The plots below demonstrated the compacted boxplots of the LLRa for all the subjects in each group for three TMS application time delays conditions, with the asterisk based on the p-values revealed from the Steel method comparisons with controlling for each group's TMS Off- Pert On condition (Figure 3.5 and Figure 3.6).

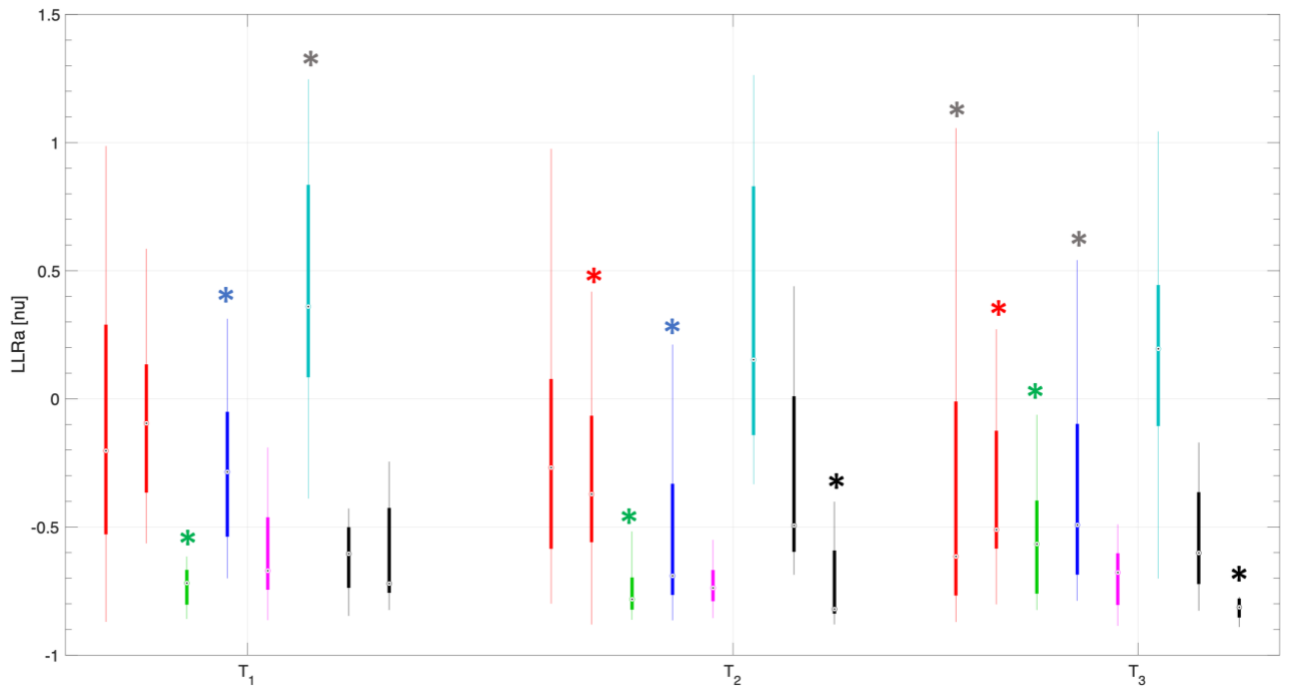


Figure 3.5 The plots for distribution of LLRa for all the subjects in group 1, for three TMS application time delays conditions. Each line shows the range with the bolded region indicates the inter quartiles range centered on the median. The asterisks denote significant results based on the Steel's method multiple comparisons test with an adjusted  $p$ -value  $< 0.0125$  and gray asterisks denote significant results at  $p < 0.05$ . The bars with the same colors are for the same subjects (repetitions). Subj 5 in T<sub>1</sub>, Subj 1 (repetition1) and Subj 3 in T<sub>3</sub> had  $p$ -values  $< 0.05$  (but  $> 0.0125$ ).

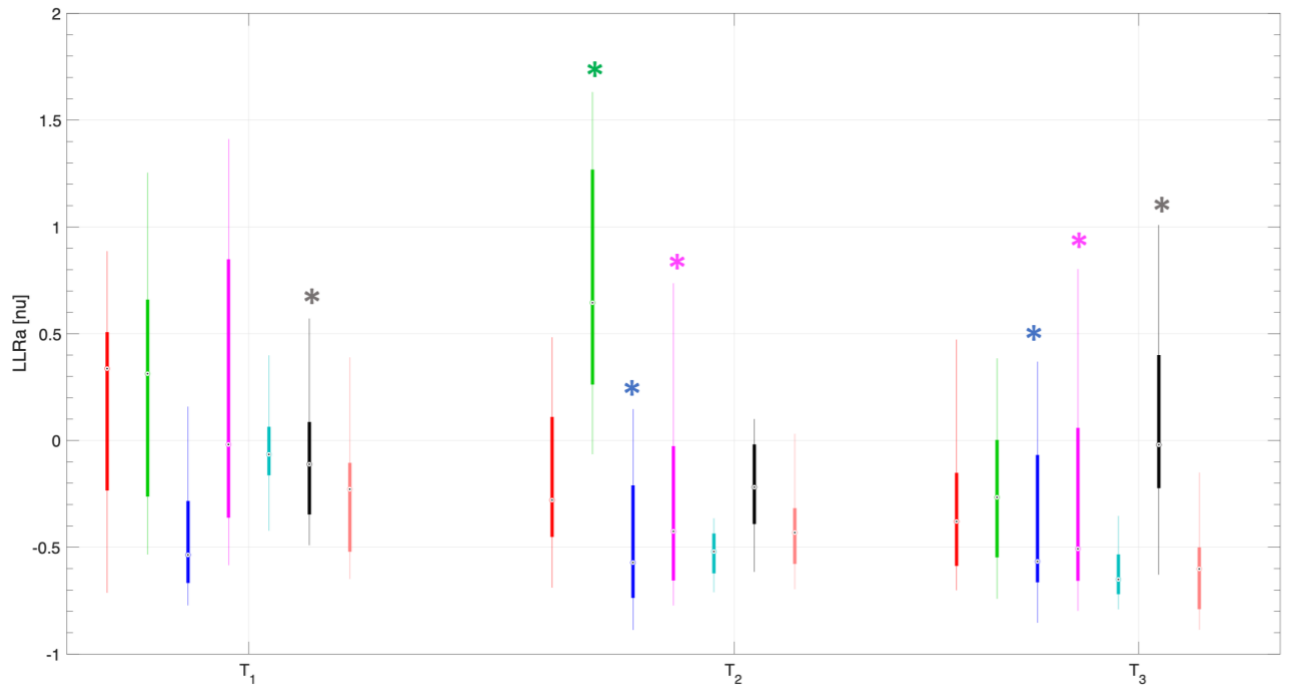


Figure 3.6 The plots for distribution of LLRa for all the subjects in group 2, for three TMS application time delays conditions. Each line shows the range with the bolded region indicates the inter quartiles range centered on the median. The asterisks denote significant results based on the Steel's method multiple comparisons test ( $p < 0.0125$ ) and gray asterisks denote significant results at  $p < 0.05$ . Subj 6 in  $T_1$  and  $T_3$  had  $p$ -value  $< 0.05$  (but  $> 0.0125$ ).

### 3.2.5 Repeatability analysis

The experiment was repeated for subject 1 and subject 6 of group 1 to check for the repeatability of the results and individual-level variance. The full factorial least square means model revealed significant modulation of the LLRa with different experimental conditions ( $p < 0.001$  for both participants). The day (repetition) and the interaction between the day and condition didn't modulate the LLRa for subject 1 ( $p = 0.97$  and  $0.55$ , respectively); however, the model revealed significant effects of both the day ( $p < 0.001$ ) and the interaction between the day and condition ( $p = 0.002$ ) for subject 6, with a greater significant reduction in LLRa in T<sub>2</sub> and T<sub>3</sub> conditions ( $p < 0.001$  and  $p = 0.032$ , respectively).

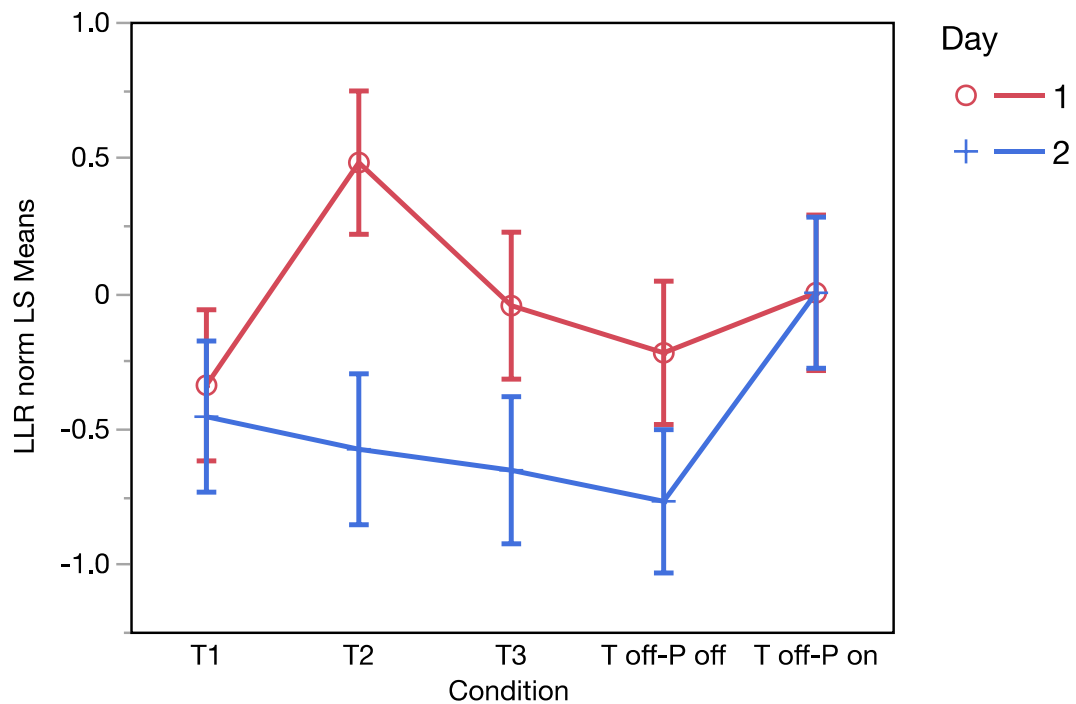


Figure 3.7 Least square means plot for two experiment repetitions for subject 6. A significant reduction in LLRa was measured in day 2 compared to day 1 of the experiment.

## Chapter 4

### CONCLUSIONS

#### 4.1 Major findings

This thesis work findings demonstrated that a subthreshold TMS signal delivered over the motor cortex can modulate the amplitude of the stretch-evoked muscle responses evoked from the wrist flexor muscle. In line with the previous studies which utilized TMS to study the neural substrates of LLR [78]–[84], our study also showed that TMS can modulate the LLR amplitude in different ways depending on the TMS signal intensity and arrival time based on the EMG activity period.

Findings showed an inhibitory effect of TMS intensity of 90%AMT with all  $T_L$  latencies on the LLRa, while  $T_1$ , the condition that MEPs occurred at the same time with the stretch (perturbation) onset, resulted in a non-significant 14.1% reduction ( $p=0.102$ ),  $T_2$  ( $T_1+ 20ms$ ) and  $T_3$  ( $T_1+ 50ms$ ) resulted in a significant reduction of 20.3% ( $p=0.008$ ), and 22.8 % ( $p=0.002$ ), respectively. While in the other group, as the TMS signal was delivered with 95%AMT intensity, a significant inhibitory modulation of LLRa was observed with  $T_3$  latency condition, which resulted in 25.3% reduction ( $p<0.001$ ), in the LLRa.  $T_2$  condition also resulted in inhibitory effect with 15.1% reduction ( $p=0.017$ ) in the LLRa. Instead,  $T_1$  condition revealed a non-significant 3.5% excitatory effect ( $p=0.912$ ), on the LLRa.

Several previous studies targeting the effects of subthreshold TMS on LLR reported non-coherent excitatory and inhibitory effects of subthreshold TMS on the LLR amplitude, but agreed that there was a significant effect of TMS pulse timing on whether the effect would be facilitatory or excitatory [78], [80], [82], [84]. Specifically, Doornik et al., 2004 [82], showed that the TMS signal with 90% of AMT over the motor cortex had an inhibitory effect, averaged around 38%, on the LLRa evoked from the tibialis anterior muscle, when TMS was administered 55–85 ms prior to LLR onset. Notably, in that study LLR onset was  $99 \pm 8$  ms after the stretch (plantar flexion) of the ankle joint. Hence, the TMS was applied around 15-45ms after the stretch onset.

On the other hand, another study in 2004 [80], reported a reduction in the LLR amplitude while TMS signal over the motor cortex was timed to induce an MEP at the SLR onset ( averaged  $22.4 \pm 3.1$  ms after the stretch onset) of the EMG activity, which was recorded from the FCR muscle. This inhibition was increased as the TMS signal increased from 90% to 140% AMT. Moreover, two other studies also evaluated how a subthreshold TMS signal over the motor cortex would modulate the LLRa evoked from FCR muscle when the extension perturbations were applied on the wrist joint [78], [84]. Ruit et al., in 2011 [84], observed a significant 20% excitatory and inhibitory effects of a subthreshold TMS signal 2-3% below the AMT on the FCR LLRa. Signals which arrived within 35 to 55 ms (average of 45 ms) after the stretch onset inhibited the LLRa, while signals with averaged arrival time of 60 ms after the stretch onset, excited the LLRa. The other study in 2015 [78], reported no inhibitory, but excitatory effects of a subthreshold TMS signal with an intensity of 96% below the AMT on the LLRa evoked from FCR muscle. These authors also found that the TMS pulses which were timed to

evoke MEPs within 60 to 90 ms after the stretch onset substantially augmented the FCR evoked LLR activity.

It is noteworthy to mention that the silent period which follows the excitatory motor evoked potential, has a various neurophysiology substrate. Importantly, the first 50 ms is widely considered to be induced due to the spinal inhibitory network, via mechanisms such as following of the hyperpolarization of the motoneurons and recurrent inhibition, but the further section of the silent period is assumed to be due to supraspinal inhibition [71]–[75]. This prolonged loss in the motor cortical output is resulted due to the activation of long-lasting GABA(B) mediated inhibition via the TMS [76], [77]. Therefore, the previous studies which applied the TMS signals after the stretch onset likely modulated the LLRa through the spinal circuits, and not supraspinal and intracortical pathways. Furthermore, based on the best of our knowledge, there is no prior study used subthreshold TMS to achieve inhibition on the LLR amplitude by relying primarily on the intracortical inhibitory effects of TMS via a silent period, with consideration of the first 50 ms spinal and following intracortical neurophysiology of silent period phenomenon to manipulate the TMS application timing, which was one of our main objectives in development of our synchronized robotic TMS-EMG system. Notably, this combination of subthreshold TMS and silent-period inhibition would be ideal to study subcortical contributions via fMRI in a future study.

In summary, our results identified two conditions (T2 and T3) that induced a significant inhibition of LLR activity in both groups, but no significant difference between groups was measured for any TMS delay levels inducing significant inhibition. Moreover, the TMS application timed to evoke MEPs 50ms before the stretch onset (condition T3) was found to have a greater inhibitory effect on the LLRa in both groups,

with both the 90% and 95% subthreshold TMS intensity. Given the known first 50ms spinal and following intracortical neurophysiology of silent period phenomenon, this time delay likely inhibited the intracortical pathways contributed to the LLRa, which is a crucial finding to be applied for our future TMS-fMRI study, with the aim of understanding and measuring the contribution of secondary pathways mainly RST to the long-latency responses.

#### **4.2 Future study**

This thesis findings showed the inhibitory effect of a subthreshold TMS signal on the LLRa, which has been shown to be able to activate intracortical inhibitory structures and does not elicit any descending volleys in the corticospinal tract [82], [86]. We found this feature of subthreshold TMS signal very crucial to be considered in our work as the findings of this thesis project will be used in our future TMS-fMRI study which, for the first time, would be the demonstration of a successful combination of TMS and fMRI to study causality of neural function in a distributed motor circuit, involving the primary motor cortex and the brainstem. These methods will be enabled utilizing our novel MR-compatible TMS device for the neuromodulation of motor circuits, which, for the first time, enables the combination of these two methods. The application of the new methods will generate new knowledge on the neural processing of long-latency muscle responses. Specifically, the identification of a causal link between neural circuits and behavior is considered one of the most important topics of investigation of modern neuroscience [90].

## REFERENCES

- [1] H. Kuypers, "Anatomy of the descending pathways.," *Handb. Physiol. Nerv. Syst. II.*, pp. 56–59, 1981.
- [2] K. Mewes and P. D. Cheney, "Facilitation and suppression of wrist and digit muscles from single rubromotoneuronal cells in the awake monkey," *J. Neurophysiol.*, vol. 66, no. 6, pp. 1965–1977, 1991.
- [3] B. Schepens and T. Drew, "Independent and convergent signals from the pontomedullary reticular formation contribute to the control of posture and movement during reaching in the cat," *J. Neurophysiol.*, vol. 92, no. 4, pp. 2217–2238, 2004.
- [4] B. Schepens and T. Drew, "Descending signals from the pontomedullary reticular formation are bilateral, asymmetric, and gated during reaching movements in the cat," *J. Neurophysiol.*, vol. 96, no. 5, pp. 2229–2252, 2006.
- [5] S. N. Baker, "The primate reticulospinal tract, hand function and functional recovery," *J. Physiol.*, vol. 589, no. 23, pp. 5603–5612, 2011.
- [6] B. Zaaimi, S. A. Edgley, D. S. Soteropoulos, and S. N. Baker, "Changes in descending motor pathway connectivity after corticospinal tract lesion in macaque monkey," *Brain*, vol. 135, no. 7, pp. 2277–2289, 2012.
- [7] C. N. Riddle, S. A. Edgley, and S. N. Baker, "Direct and indirect connections with upper limb motoneurons from the primate reticulospinal tract," *J. Neurosci.*, vol. 29, no. 15, pp. 4993–4999, 2009.
- [8] A. G. Davidson, M. H. Schieber, and J. A. Buford, "Bilateral Spike-Triggered Average Effects in Arm and Shoulder Muscles from the Monkey Pontomedullary Reticular Formation," *J. Neurosci.*, vol. 27, no. 30, pp. 8053–8058, 2007, doi: 10.1523/JNEUROSCI.0040-07.2007.
- [9] S. Choudhury *et al.*, "The relationship between enhanced reticulospinal outflow and upper limb function in chronic stroke patients," *Neurorehabil. Neural Repair*, vol. 33, no. 5, pp. 375–383, 2019.
- [10] J. G. McPherson, A. Chen, M. D. Ellis, J. Yao, C. J. Heckman, and J. P. A. Dewald, "Progressive recruitment of contralesional cortico-reticulospinal pathways drives motor impairment post stroke," *J. Physiol.*, vol. 596, no. 7, pp. 1211–1225, 2018.

- [11] S. Li, “Spasticity, motor recovery, and neural plasticity after stroke,” *Front. Neurol.*, vol. 8, p. 120, 2017.
- [12] Y.-T. Chen, S. Li, P. Zhou, and S. Li, “A startling acoustic stimulation (SAS)-TMS approach to assess the reticulospinal system in healthy and stroke subjects,” *J. Neurol. Sci.*, vol. 399, pp. 82–88, 2019.
- [13] M. Owen, C. Ingo, and J. Dewald, “Upper extremity motor impairments and microstructural changes in bulbospinal pathways in chronic hemiparetic stroke,” *Front. Neurol.*, vol. 8, p. 257, 2017.
- [14] S. Li, Y.-T. Chen, G. E. Francisco, P. Zhou, and W. Z. Rymer, “A unifying pathophysiological account for post-stroke spasticity and disordered motor control,” *Front. Neurol.*, vol. 10, p. 468, 2019.
- [15] E. Mtui, G. Gruener, and M. J. T. FitzGerald, *Clinical Neuroanatomy and Neuroscience E-Book*. Elsevier Health Sciences, 2011.
- [16] B. E. B. Gjelsvik and L. Syre, *The Bobath concept in adult neurology*. Thieme Stuttgart, 2008.
- [17] C. Trompetto *et al.*, “Pathophysiology of spasticity: implications for neurorehabilitation,” *Biomed Res. Int.*, vol. 2014, 2014.
- [18] A. G. Davidson and J. A. Buford, “Motor outputs from the primate reticular formation to shoulder muscles as revealed by stimulus-triggered averaging,” *J. Neurophysiol.*, vol. 92, no. 1, pp. 83–95, 2004.
- [19] J. A. Buford, “Reticulospinal System,” in *Encyclopedia of Neuroscience*, Elsevier, 2009, pp. 151–158.
- [20] E. J. Benjamin *et al.*, “Heart disease and stroke statistics—2018 update: a report from the American Heart Association,” *Circulation*, vol. 137, no. 12, pp. e67–e492, 2018.
- [21] P. Brown, “Pathophysiology of spasticity,” *J. Neurol. Neurosurg. Psychiatry*, vol. 57, no. 7, p. 773, 1994.
- [22] G. Sheean, “The pathophysiology of spasticity,” *Eur. J. Neurol.*, vol. 9, pp. 3–9, 2002.
- [23] S. Li and G. E. Francisco, “New insights into the pathophysiology of post-stroke spasticity,” *Front. Hum. Neurosci.*, vol. 9, p. 192, 2015.
- [24] R. R. Young, “Spasticity: a review,” *Neurology*, vol. 44, no. 11 Suppl 9, pp.

S12-20, 1994.

- [25] K. D'Ardenne, S. M. McClure, L. E. Nystrom, and J. D. Cohen, "BOLD responses reflecting dopaminergic signals in the human ventral tegmental area," *Science (80-. )*, vol. 319, no. 5867, pp. 1264–1267, 2008.
- [26] S. Katyal, S. Zughni, C. Greene, and D. Ress, "Topography of covert visual attention in human superior colliculus," *J. Neurophysiol.*, vol. 104, no. 6, pp. 3074–3083, 2010.
- [27] L. A. Henderson and V. G. Macefield, "Functional imaging of the human brainstem during somatosensory input and autonomic output," *Front. Hum. Neurosci.*, vol. 7, p. 569, 2013.
- [28] S. Katyal and D. Ress, "Endogenous attention signals evoked by threshold contrast detection in human superior colliculus," *J. Neurosci.*, vol. 34, no. 3, pp. 892–900, 2014.
- [29] E.-D. X. Cifu, "Braddom's Physical Medicine and Rehabilitation E-Book, livre ebook," 2015.
- [30] I. L. Kurtzer, "Long-latency reflexes account for limb biomechanics through several supraspinal pathways," vol. 8, no. January, pp. 1–19, 2015, doi: 10.3389/fnint.2014.00099.
- [31] K.-E. Hagbarth, J. V Hägglund, E. U. Wallin, and R. R. Young, "Grouped spindle and electromyographic responses to abrupt wrist extension movements in man," *J. Physiol.*, vol. 312, no. 1, pp. 81–96, 1981.
- [32] R. G. Lee and W. G. Tatton, "Long latency reflexes to imposed displacements of the human wrist: Dependence on duration of movement," *Exp. Brain Res.*, vol. 45, no. 1–2, pp. 207–216, 1982, doi: 10.1007/BF00235780.
- [33] G. N. Lewis, E. J. Perreault, and C. D. MacKinnon, "The influence of perturbation duration and velocity on the long-latency response to stretch in the biceps muscle," *Exp. Brain Res.*, vol. 163, no. 3, pp. 361–369, 2005, doi: 10.1007/s00221-004-2182-9.
- [34] J. Schuurmans, E. De Vlught, A. C. Schouten, C. G. M. Meskers, J. H. De Groot, and F. C. T. Van Der Helm, "The monosynaptic Ia afferent pathway can largely explain the stretch duration effect of the long latency M2 response," *Exp. brain Res.*, vol. 193, no. 4, pp. 491–500, 2009.
- [35] I. Kurtzer, J. A. Pruszynski, and S. H. Scott, "Long-latency and voluntary

responses to an arm displacement can be rapidly attenuated by perturbation offset,” *J. Neurophysiol.*, vol. 103, no. 6, pp. 3195–3204, 2010.

- [36] A. Hendrie and R. G. Lee, “Selective effects of vibration on human spinal and long-loop reflexes,” *Brain Res.*, vol. 157, no. 2, pp. 369–375, 1978.
- [37] D. C. LAWRENCE and H. KUYPEFLS, “1968. The functional organization of the motor system in monkey. 11. The effects of lesions of the descending brain-stem pathways,” *Brain*, vol. 81, p. 1536.
- [38] C. G. M. Meskers, A. C. Schouten, M. M. L. Rich, J. H. De Groot, J. Schuurmans, and J. H. Arendzen, “Tizanidine does not affect the linear relation of stretch duration to the long latency M2 response of m. flexor carpi radialis,” *Exp. brain Res.*, vol. 201, no. 4, pp. 681–688, 2010.
- [39] A. J. Suminski, S. M. Rao, K. M. Mosier, and R. A. Scheidt, “Neural and electromyographic correlates of wrist posture control,” *J. Neurophysiol.*, vol. 97, no. 2, pp. 1527–1545, 2007.
- [40] R. Shadmehr and F. A. Mussa-Ivaldi, “Adaptive representation of dynamics during learning of a motor task,” *J. Neurosci.*, vol. 14, no. 5, pp. 3208–3224, 1994.
- [41] H. Asanuma, “Recent developments in the study of the columnar arrangement of neurons within the motor cortex,” *Physiol. Rev.*, vol. 55, no. 2, pp. 143–156, 1975.
- [42] B. Conrad, J. Meyer-Lohmann, K. Matsunami, and V. B. Brooks, “Precentral unit activity following torque pulse injections into elbow movements,” *Brain Res.*, vol. 94, no. 2, pp. 219–236, 1975.
- [43] E. V. Evarts and J. Tanji, “Reflex and intended responses in motor cortex pyramidal tract neurons of monkey,” *J. Neurophysiol.*, vol. 39, no. 5, pp. 1069–1080, 1976.
- [44] T. M. Herter, T. Korbelt, and S. H. Scott, “Comparison of neural responses in primary motor cortex to transient and continuous loads during posture,” *J. Neurophysiol.*, vol. 101, no. 1, pp. 150–163, 2009.
- [45] P. D. Cheney, E. E. Fetz, and K. Mewes, “Neural mechanisms underlying corticospinal and rubrospinal control of limb movements,” *Prog. Brain Res.*, vol. 87, pp. 213–252, 1991.
- [46] P. Hammond, “The influence of prior instruction to the subject on an apparently

- involuntary neuromuscular response,” *J. Physiol.*, vol. 132, pp. 17–18, 1956.
- [47] J. C. Rothwell, M. M. Traub, and C. D. Marsden, “Influence of voluntary intent on the human long-latency stretch reflex,” *Nature*, vol. 286, no. 5772, pp. 496–498, 1980.
- [48] G. N. Lewis, C. D. MacKinnon, and E. J. Perreault, “The effect of task instruction on the excitability of spinal and supraspinal reflex pathways projecting to the biceps muscle,” *Exp. Brain Res.*, vol. 174, no. 3, pp. 413–425, 2006, doi: 10.1007/s00221-006-0475-x.
- [49] J. A. Pruszynski, I. Kurtzer, and S. H. Scott, “The long-latency reflex is composed of at least two functionally independent processes,” *J. Neurophysiol.*, vol. 106, no. 1, pp. 449–459, 2011, doi: 10.1152/jn.01052.2010.
- [50] J. Valls-Solé, J. C. Rothwell, F. Goulart, G. Cossu, and E. Munoz, “Patterned ballistic movements triggered by a startle in healthy humans,” *J. Physiol.*, vol. 516, no. 3, pp. 931–938, 1999.
- [51] A. N. Carlsen, D. Maslovat, M. Y. Lam, R. Chua, and I. M. Franks, “Considerations for the use of a startling acoustic stimulus in studies of motor preparation in humans,” *Neurosci. Biobehav. Rev.*, vol. 35, no. 3, pp. 366–376, 2011.
- [52] J. S. Yeomans, L. Li, B. W. Scott, and P. W. Frankland, “Tactile, acoustic and vestibular systems sum to elicit the startle reflex,” *Neurosci. Biobehav. Rev.*, vol. 26, no. 1, pp. 1–11, 2002.
- [53] C. F. Honeycutt and E. J. Perreault, “Planning of ballistic movement following stroke: insights from the startle reflex,” 2012.
- [54] J. Nonnekes *et al.*, “StartReact restores reaction time in HSP: evidence for subcortical release of a motor program,” *J. Neurosci.*, vol. 34, no. 1, pp. 275–281, 2014.
- [55] V. J. Ravichandran, C. F. Honeycutt, J. Shemmell, and E. J. Perreault, “Instruction-dependent modulation of the long-latency stretch reflex is associated with indicators of startle,” *Exp. brain Res.*, vol. 230, no. 1, pp. 59–69, 2013.
- [56] K. Lingenhöhl and E. Friauf, “Giant neurons in the caudal pontine reticular formation receive short latency acoustic input: an intracellular recording and HRP-study in the rat,” *J. Comp. Neurol.*, vol. 325, no. 4, pp. 473–492, 1992.

- [57] K. Lingenhohl and E. Friauf, “Giant neurons in the rat reticular formation: a sensorimotor interface in the elementary acoustic startle circuit?,” *J. Neurosci.*, vol. 14, no. 3, pp. 1176–1194, 1994.
- [58] A. Mitani, K. Ito, Y. Mitani, and R. W. McCarley, “Morphological and electrophysiological identification of gigantocellular tegmental field neurons with descending projections in the cat: I. Pons,” *J. Comp. Neurol.*, vol. 268, no. 4, pp. 527–545, 1988.
- [59] A. Zonnino, A. J. Farrens, D. Ress, and F. Sergi, “StretchfMRI: A novel technique to quantify the contribution of the reticular formation to long-latency responses via fMRI,” in *IEEE International Conference on Rehabilitation Robotics*, 2019, vol. 2019-June, pp. 1247–1253, doi: 10.1109/ICORR.2019.8779451.
- [60] A. Zonnino, A. J. Farrens, D. Ress, and F. Sergi, “Measurement of stretch-evoked brainstem function using fMRI,” *Sci. Rep.*, vol. 11, no. 1, pp. 1–21, 2021.
- [61] A. T. Barker, R. Jalinous, and I. L. Freeston, “Non-invasive magnetic stimulation of human motor cortex,” *Lancet*, vol. 325, no. 8437, pp. 1106–1107, 1985.
- [62] S. Groppa *et al.*, “A practical guide to diagnostic transcranial magnetic stimulation: report of an IFCN committee,” *Clin. Neurophysiol.*, vol. 123, no. 5, pp. 858–882, 2012.
- [63] S. Yang *et al.*, “3D realistic head model simulation based on transcranial magnetic stimulation,” in *2006 International Conference of the IEEE Engineering in Medicine and Biology Society*, 2006, pp. 6469–6472.
- [64] M. C. Ridding and J. C. Rothwell, “Is there a future for therapeutic use of transcranial magnetic stimulation?,” *Nat. Rev. Neurosci.*, vol. 8, no. 7, pp. 559–567, 2007.
- [65] P. J. Maccabee, V. E. Amassian, L. P. Eberle, and R. Q. Cracco, “Magnetic coil stimulation of straight and bent amphibian and mammalian peripheral nerve in vitro: locus of excitation,” *J. Physiol.*, vol. 460, no. 1, pp. 201–219, 1993.
- [66] S. Groppa *et al.*, “The human dorsal premotor cortex facilitates the excitability of ipsilateral primary motor cortex via a short latency cortico-cortical route,” *Hum. Brain Mapp.*, vol. 33, no. 2, pp. 419–430, 2012.
- [67] P. M. Rossini *et al.*, “Non-invasive electrical and magnetic stimulation of the

brain, spinal cord, roots and peripheral nerves: basic principles and procedures for routine clinical and research application. An updated report from an IFCN Committee,” *Clin. Neurophysiol.*, vol. 126, no. 6, pp. 1071–1107, 2015.

- [68] J. E. Butler, N. C. Petersen, R. D. Herbert, S. C. Gandevia, and J. L. Taylor, “Origin of the low-level EMG during the silent period following transcranial magnetic stimulation,” *Clin. Neurophysiol.*, vol. 123, no. 7, pp. 1409–1414, 2012.
- [69] P. A. Merton, “The silent period in a muscle of the human hand,” *J. Physiol.*, vol. 114, no. 1–2, pp. 183–198, 1951.
- [70] P. A. Merton, “Significance of the ‘silent period’ of muscles,” *Nature*, vol. 166, no. 4226, pp. 733–734, 1950.
- [71] M. Inghilleri, A. Berardelli, G. Cruccu, and M. Manfredi, “Silent period evoked by transcranial stimulation of the human cortex and cervicomedullary junction,” *J. Physiol.*, vol. 466, no. 1, pp. 521–534, 1993.
- [72] R. Cantello, M. Gianelli, C. Civardi, and R. Mutani, “Magnetic brain stimulation: the silent period after the motor evoked potential,” *Neurology*, vol. 42, no. 10, p. 1951, 1992.
- [73] P. Fuhr, R. Agostino, and M. Hallett, “Spinal motor neuron excitability during the silent period after cortical stimulation,” *Electroencephalogr. Clin. Neurophysiol. Potentials Sect.*, vol. 81, no. 4, pp. 257–262, 1991.
- [74] S. A. Wilson, R. J. Lockwood, G. W. Thickbroom, and F. L. Mastaglia, “The muscle silent period following transcranial magnetic cortical stimulation,” *J. Neurol. Sci.*, vol. 114, no. 2, pp. 216–222, 1993.
- [75] U. Ziemann, J. Netz, A. Szelényi, and V. Hömberg, “Spinal and supraspinal mechanisms contribute to the silent period in the contracting soleus muscle after transcranial magnetic stimulation of human motor cortex,” *Neurosci. Lett.*, vol. 156, no. 1–2, pp. 167–171, 1993.
- [76] M. N. McDonnell, Y. Orekhov, and U. Ziemann, “The role of GABA B receptors in intracortical inhibition in the human motor cortex,” *Exp. Brain Res.*, vol. 173, no. 1, pp. 86–93, 2006.
- [77] N. Lang, E. Sueske, A. Hasan, W. Paulus, and F. Tergau, “Pregabalin Exerts Oppositional Effects on Different Inhibitory Circuits in Human Motor Cortex: A Double-blind, Placebo-controlled Transcranial Magnetic Stimulation Study,” *Epilepsia*, vol. 47, no. 5, pp. 813–819, 2006.

- [78] M. J. L. Perenboom, M. Van de Ruit, J. H. De Groot, A. C. Schouten, and C. G. M. Meskers, “Evidence for sustained cortical involvement in peripheral stretch reflex during the full long latency reflex period,” *Neurosci. Lett.*, vol. 584, pp. 214–218, 2015.
- [79] H. B. Meziane, L. Spieser, J. Pailhous, and M. Bonnard, “Corticospinal control of wrist muscles during expectation of a motor perturbation: a transcranial magnetic stimulation study,” *Behav. Brain Res.*, vol. 198, no. 2, pp. 459–465, 2009.
- [80] G. N. Lewis, M. A. Polych, and W. D. Byblow, “Proposed cortical and sub-cortical contributions to the long-latency stretch reflex in the forearm,” *Exp. Brain Res.*, vol. 156, no. 1, pp. 72–79, 2004, doi: 10.1007/s00221-003-1767-z.
- [81] J. Shemmell, J. H. An, and E. J. Perreault, “The differential role of motor cortex in stretch reflex modulation induced by changes in environmental mechanics and verbal instruction,” *J. Neurosci.*, vol. 29, no. 42, pp. 13255–13263, 2009.
- [82] J. van Doornik, Y. Masakado, T. Sinkjaer, and J. B. Nielsen, “The suppression of the long-latency stretch reflex in the human tibialis anterior muscle by transcranial magnetic stimulation,” *Exp. brain Res.*, vol. 157, no. 3, pp. 403–406, 2004.
- [83] J. Fox and J. Shemmell, “The ipsilateral motor cortex does not contribute to long-latency stretch reflex amplitude at the wrist,” *Brain Behav.*, vol. 4, no. 1, pp. 60–69, 2014.
- [84] M. L. Van de Ruit, “Studying cortical involvement in the long latency stretch reflex response using subthreshold TMS,” 2011.
- [85] T. Kujirai *et al.*, “Corticocortical inhibition in human motor cortex.,” *J. Physiol.*, vol. 471, no. 1, pp. 501–519, 1993.
- [86] V. Di Lazzaro *et al.*, “Magnetic transcranial stimulation at intensities below active motor threshold activates intracortical inhibitory circuits,” *Exp. brain Res.*, vol. 119, no. 2, pp. 265–268, 1998.
- [87] J. Weinman, P. Arfa-Fatollahkhani, A. Zonnino, R. C. Nikonowicz, and F. Sergi, “Effects of Perturbation Velocity, Direction, Background Muscle Activation, and Task Instruction on Long-Latency Responses Measured From Forearm Muscles,” *Front. Hum. Neurosci.*, vol. 15, p. 178, 2021.
- [88] E. Wassermann, C. Epstein, U. Ziemann, and V. Walsh, *Oxford handbook of transcranial stimulation*. Oxford University Press, 2008.

- [89] N. Petersen, L. O. D. Christensen, H. Morita, T. Sinkjær, and J. Nielsen, “Evidence that a transcortical pathway contributes to stretch reflexes in the tibialis anterior muscle in man,” *J. Physiol.*, vol. 512, no. 1, pp. 267–276, 1998.
- [90] I. E. Marinescu, P. N. Lawlor, and K. P. Kording, “Quasi-experimental causality in neuroscience and behavioural research,” *Nat. Hum. Behav.*, vol. 2, no. 12, pp. 891–898, 2018.
- [91] L. Richter, G. Neumann, S. Oung, A. Schweikard, and P. Trillenber, “Optimal coil orientation for transcranial magnetic stimulation,” *PLoS One*, vol. 8, no. 4, p. e60358, 2013.
- [92] M. Hallett, “Transcranial magnetic stimulation: a primer,” *Neuron*, vol. 55, no. 2, pp. 187–199, 2007.
- [93] P. M. Rossini, M. D. Caramia, C. Iani, M. T. Desiato, G. Sciarretta, and G. Bernardi, “Magnetic transcranial stimulation in healthy humans: influence on the behavior of upper limb motor units,” *Brain Res.*, vol. 676, no. 2, pp. 314–324, 1995.
- [94] J. Škarabot, R. N. O. Mesquita, C. G. Brownstein, and P. Ansdell, “Myths and Methodologies: How loud is the story told by the transcranial magnetic stimulation-evoked silent period?,” *Exp. Physiol.*, vol. 104, no. 5, pp. 635–642, 2019.
- [95] A. Wolters, U. Ziemann, R. Benecke, E. M. Wasserman, C. M. Epstein, and U. Ziemann, “The cortical silent period,” in *The Oxford handbook of transcranial stimulation*, Oxford University Press, 2008, pp. 91–102.
- [96] P. E. McKight and J. Najab, “Kruskal-wallis test,” *corsini Encycl. Psychol.*, p. 1, 2010.
- [97] M. Neuhäuser and F. Bretz, “Nonparametric all-pairs multiple comparisons,” *Biometrical J. J. Math. Methods Biosci.*, vol. 43, no. 5, pp. 571–580, 2001.
- [98] M. Stuart and J. L. Taylor, “Subthreshold transcranial magnetic stimulation during the long latency component of the cutaneomotor reflex,” *Exp. brain Res.*, vol. 170, no. 3, pp. 285–294, 2006.

# Appendix A

## T1 STRUCTURAL SCAN REPORT

SIEMENS MAGNETOM Prisma

\\USER\Sergi\EMG\TMS Structural\T1 MPRAGE ISO .7MM_ 2avg	
TA: 16:35 PM: REF Voxel size: 0.7x0.7x0.7 mmPAT: 2 Rel. SNR: 1.00 : tfl	

### Properties

Prio recon	Off
Load images to viewer	On
Inline movie	Off
Auto store images	On
Load images to stamp segments	On
Load images to graphic segments	On
Auto open inline display	Off
Auto close inline display	Off
Start measurement without further preparation	Off
Wait for user to start	On
Start measurements	Single measurement

### Resolution - iPAT

PAT mode	GRAPPA
Accel. factor PE	2
Ref. lines PE	24
Accel. factor 3D	1
Reference scan mode	Integrated

### Resolution - Filter Image

Image Filter	Off
Distortion Corr.	Off
Prescan Normalize	On
Unfiltered images	Off
Normalize	Off
B1 filter	Off

### Routine

Slab group	1
Slabs	1
Dist. factor	50 %
Position	R1.8 A28.3 H44.2 mm
Orientation	Sagittal
Phase enc. dir.	A >> P
AutoAlign	Head > Brain
Phase oversampling	25 %
Slice oversampling	25.0 %
Slices per slab	256
FoV read	210 mm
FoV phase	100.0 %
Slice thickness	0.70 mm
TR	2600.0 ms
TE	4.64 ms
Averages	2
Concatenations	1
Filter	Prescan Normalize
Coil elements	HC1-7;NC1

### Resolution - Filter Rawdata

Raw filter	Off
Elliptical filter	Off

### Geometry - Common

Slab group	1
Slabs	1
Dist. factor	50 %
Position	R1.8 A28.3 H44.2 mm
Orientation	Sagittal
Phase enc. dir.	A >> P
Slice oversampling	25.0 %
Slices per slab	256
FoV read	210 mm
FoV phase	100.0 %
Slice thickness	0.70 mm
TR	2600.0 ms
Multi-slice mode	Single shot
Series	Interleaved
Concatenations	1

### Contrast - Common

TR	2600.0 ms
TE	4.64 ms
Magn. preparation	Non-sel. IR
TI	1310 ms
Flip angle	9 deg
Fat suppr.	None
Water suppr.	None

### Geometry - AutoAlign

Slab group	1
Position	R1.8 A28.3 H44.2 mm
Orientation	Sagittal
Phase enc. dir.	A >> P
AutoAlign	Head > Brain
Initial Position	R1.8 A28.3 H44.2
R	1.8 mm
A	28.3 mm
H	44.2 mm
Initial Rotation	0.00 deg
Initial Orientation	Sagittal

### Contrast - Dynamic

Averages	2
Averaging mode	Long term
Reconstruction	Magnitude
Measurements	1
Multiple series	Off

### Geometry - Navigator

### Geometry - Tim Planning Suite

Set-n-Go Protocol	Off
Table position	H
Table position	0 mm
Inline Composing	Off

### Resolution - Common

FoV read	210 mm
FoV phase	100.0 %
Slice thickness	0.70 mm
Base resolution	288
Phase resolution	100 %
Slice resolution	74 %
Phase partial Fourier	Off
Slice partial Fourier	Off
Interpolation	Off

### System - Miscellaneous

Positioning mode	REF
Table position	H
Table position	0 mm

SIEMENS MAGNETOM Prisma

**System - Miscellaneous**

MSMA	S - C - T
Sagittal	R >> L
Coronal	A >> P
Transversal	F >> H
Coil Combine Mode	Adaptive Combine
Save uncombined	Off
Matrix Optimization	Off
AutoAlign	Head > Brain
Coil Select Mode	Default

**System - Adjustments**

B0 Shim mode	Standard
B1 Shim mode	TrueForm
Adjust with body coil	Off
Confirm freq. adjustment	Off
Assume Dominant Fat	Off
Assume Silicone	Off
Adjustment Tolerance	Auto

**System - Adjust Volume**

Position	R1.8 A28.3 H44.2 mm
Orientation	Sagittal
Rotation	0.00 deg
A >> P	210 mm
F >> H	210 mm
R >> L	180 mm
Reset	Off

**System - pTx Volumes**

B1 Shim mode	TrueForm
Excitation	Non-sel.

**System - Tx/Rx**

Frequency 1H	123.259100 MHz
Correction factor	1
Gain	Low
Img. Scale Cor.	1.000
Reset	Off
? Ref. amplitude 1H	0.000 V

**Physio - Signal1**

1st Signal/Mode	None
TR	2600.0 ms
Concatenations	1

**Physio - Cardiac**

Magn. preparation	Non-sel. IR
T1	1310 ms
Fat suppr.	None
Dark blood	Off
FoV read	210 mm
FoV phase	100.0 %
Phase resolution	100 %

**Physio - PACE**

Resp. control	Off
Concatenations	1

**Inline - Common**

Subtract	Off
Measurements	1
StdDev	Off
Save original images	On

**Inline - MIP**

MIP-Sag	Off
MIP-Cor	Off
MIP-Tra	Off
MIP-Time	Off
Save original images	On

**Inline - Composing**

Inline Composing	Off
Distortion Corr.	Off

**Inline - MapIt**

Save original images	On
MapIt	None
Flip angle	9 deg
Measurements	1
TR	2600.0 ms
TE	4.64 ms

**Sequence - Part 1**

Introduction	On
Dimension	3D
Elliptical scanning	Off
Reordering	Linear
Asymmetric echo	Off
Flow comp.	No
Multi-slice mode	Single shot
Echo spacing	10.9 ms
Bandwidth	140 Hz/Px

**Sequence - Part 2**

RF pulse type	Fast
Gradient mode	Normal
Excitation	Non-sel.
RF spoiling	On
Incr. Gradient spoiling	Off
Turbo factor	236

**Sequence - Assistant**

Mode	Off
------	-----

## Appendix B

### IRB/HUMAN SUBJECTS APPROVAL



**Institutional Review Board**  
210H Hulihan Hall  
Newark, DE 19716  
Phone: 302-831-2137  
Fax: 302-831-2828

DATE: February 11, 2021

TO: Fabrizio Sergi  
FROM: University of Delaware IRB

STUDY TITLE: [1545543-2] Use of simultaneous TMS and fMRI to identify causality in human sensorimotor function

SUBMISSION TYPE: Continuing Review/Progress Report

ACTION: APPROVED

APPROVAL DATE: February 11, 2021

EXPIRATION DATE: February 18, 2022

REVIEW TYPE: Expedited Review

REVIEW CATEGORY: Expedited review category # (8)(b)

Thank you for your Continuing Review/Progress Report submission to the University of Delaware Institutional Review Board (UD IRB). The UD IRB has reviewed and APPROVED the proposed research and submitted documents via Expedited Review in compliance with the pertinent federal regulations.

As the Principal Investigator for this study, you are responsible for and agree that:

- All research must be conducted in accordance with the protocol and all other study forms as approved in this submission. Any revisions to the approved study procedures or documents must be reviewed and approved by the IRB prior to their implementation. Please use the UD amendment form to request the review of any changes to approved study procedures or documents.
- Informed consent is a process that must allow prospective participants sufficient opportunity to discuss and consider whether to participate. IRB-approved and stamped consent documents must be used when enrolling participants and a written copy shall be given to the person signing the informed consent form.
- Unanticipated problems, serious adverse events involving risk to participants, and all non-compliance issues must be reported to this office in a timely fashion according with the UD requirements for reportable events. All sponsor reporting requirements must also be followed.

Oversight of this study by the UD IRB REQUIRES the submission of a CONTINUING REVIEW seeking the renewal of this IRB approval, which will expire on February 18, 2022. A continuing review/progress report form and up-to-date copies of the protocol form and all other approved study materials must be submitted to the UD IRB at least 45 days prior to the expiration date to allow for the required IRB review of that report.

If you have any questions, please contact the UD IRB Office at (302) 831-2137 or via email at [hsrb-research@udel.edu](mailto:hsrb-research@udel.edu). Please include the study title and reference number in all correspondence with this office.